AD A070909

15, March, 1979

(12) LEVEL II

SC

ADVANCED OPTICAL CERAMICS - PHASE I

ONR CONTRACT NO. N00014-78-C-0466

THIRD QUARTERLY R&D STATUS REPORT

REPORTING PERIOD 1 DECEMBER 1978 THROUGH 28 FEBRUARY 1979

CONTRACT MONITOR: DR. A. M. DINESS
OFFICE OF NAVAL RESEARCH

PROGRAM MANAGER: DR. SOLOMON MUSIKANT
GENERAL ELECTRIC COMPANY
RE-ENTRY & ENVIRONMENTAL
SYSTEMS DIVISION
3198 CHESTNUT STREET
PHILADELPHIA, PENNSYLVANIA 19101

DDC FILE COPY

The views and conclusions contained in this document are those of the authors and should not be interpreted as necessarily representing the official policies, either expressed or implied, of the Defense Advanced Research Projects Agency or the U.S.Government.

DISTRIBUTION STATEMENT A
Approved for public release;
Distribution Unlimited

DDC
RECEIVED
JUL 9 1979
B

GENERAL ELECTRIC
Re-entry & Environmental Systems Division
PHILADELPHIA, PENNSYLVANIA

79 05 09 019

SECURITY CLASSIFICATION OF THIS PAGE (When Data Entered)

REPORT DOCUMENTATION PAGE

READ INSTRUCTIONS BEFORE COMPLETING FORM

1 REPORT NUMBER: N00014-78-C-0466

2. GOVT ACCESSION NO.

3. RECIPIENT'S CATALOG NUMBER

4 TITLE (and Subtitle): Advanced Optical Ceramics • Phase "1" Third Quarterly R&D Status Report

5. TYPE OF REPORT & PERIOD COVERED: Technical Dec.1, 1978 thru Feb.28, 1979

6. PERFORMING ORG. REPORT NUMBER

7 AUTHOR(s): S. Musikant, R.A.Tanzilli, J.J.Gebhardt, H.W.Rauch, Sr., A.Gatti, R.J.Charles, S. Prochazka, G.A.Slack, R.M.Cannon, W.B.White

8. CONTRACT OR GRANT NUMBER(s): N00014-78-C-0466; DARPA Order [redacted]3387

9 PERFORMING ORGANIZATION NAME AND ADDRESS: GENERAL ELECTRIC COMPANY, RESD, 3198 Chestnut Street, Philadelphia, Penna. 19101

10. PROGRAM ELEMENT, PROJECT, TASK AREA & WORK UNIT NUMBERS

11 CONTROLLING OFFICE NAME AND ADDRESS: Office of Naval Research, 800 N. Quincy Street, Arlington, Virginia 22217

12. REPORT DATE: March [redacted], 1979

13. NUMBER OF PAGES: 114p.

14 MONITORING AGENCY NAME & ADDRESS (if different from Controlling Office)

15. SECURITY CLASS. (of this report): UNCLASSIFIED

15a. DECLASSIFICATION/DOWNGRADING SCHEDULE

16 DISTRIBUTION STATEMENT (of this Report)

DISTRIBUTION STATEMENT A
Approved for public release;
Distribution Unlimited

17 DISTRIBUTION STATEMENT (of the abstract entered in Block 20, if different from Report)

Quarterly research and development status report, no. 3, 1 Dec 78-28 Feb 79 on Phase 1,

18 SUPPLEMENTARY

DDC RECEIVED JUL 9 1979 B

19 KEY WORDS (Continue on reverse side if necessary and identify by block number)

IR domes, radome, missile, ceramics, antenna window, window, absorption coefficients.

20 ABSTRACT (Continue on reverse side if necessary and identify by block number)

The objective of this study is to identify and develop revolutionary advanced material suitable for electro-optical/electro-magnetic (EO/EM) windows, IR dome and radomes capable of meeting mission requirements anticipated for the 1990 decade and beyond.

This contract is a follow-on to an earlier study, Advanced

DD FORM 1 JAN 73 1473 EDITION OF 1 NOV 65 IS OBSOLETE

SECURITY CLASSIFICATION OF THIS PAGE (When Data Entered)

404884

79 05 09 019

Optical Ceramics - Phase "O", ONR Contract No. N00014-77-C-0649, Reference I.

During the third reporting period experimental work was directed at synthesis and characterization of the candidate window materials (Task 1.0). Synthesis was initiated and continued as indicated on Table 1.

The toughness enhancement study ~~(Task 2.0)~~ and the optical modelling ~~(Task 4.0)~~ continue to indicate the feasibility of toughening of optical materials. Refinements in the scattering model provided a quantitative relationship between the second phase toughener particle size - index of refraction requirement. In conjunction with known equilibria data, identification was made of the most feasible toughened systems for windows and enclosures. The most interesting candidates in this category are: (a) cubic stabilized ZrO_2/ unstabilized ZrO_2;

(b) (Al_2O_3-Cr_2O_3) solid solution/unstabilized ZrO_2.

because in both of these cases the index of refraction of the second phase particle is anticipated to match closely that of the matrix.

A systematic evaluation of potential new candidates ~~(Task 5.0)~~ was made and a theory for prediction of low coefficient of thermal expansion crystals was developed. This study identified, among others, the β' sialon ceramics as an important category.

Beta'

SUMMARY INFORMATION

ONR CONTRACT NUMBER: N00014-78-C-0466

ARPA ORDER NUMBER: 3387, Amendment No. 3

CONTRACTOR: General Electric Company
Re-entry & Environmental Systems Division

CONTRACT DATE: 1 June 1978

CONTRACT AMOUNT: $689,819

CONTRACT EXPIRATION DATE: 31 July 1979

SHORT TITLE OF WORK: AOC-ø I

PROGRAM MANAGER AND
PRINCIPAL INVESTIGATOR: S. Musikant
GE-RESD
Philadelphia, Pa. 19101
(215) 823-4942

PRINCIPAL SCIENTISTS: R. A. Tanzilli GE-RESD
(215) 962-6070

J. J. Gebhardt
(215) 962-1227

H. W. Rauch, Sr. GE-SD/SSL
(215) 962-2195

A. Gatti
(215) 962-2195

R. J. Charles GE-CRD
(518) 385-8605

S. Prochazca
(518) 385-8534

G. A. Slack
(518) 385-8601

Accession For
NTIS GRA&I ☑
DDC TAB ☐
Unannounced ☐
Justification
PER LETTER
By
Distribution/
Availability Codes
Dist | Avail and/or special
A

PRINCIPAL SCIENTISTS: (continued)	R. M. Cannon, Jr. (617) 253-6471	MIT
	W. B. White (814) 865-1152	Penn State University
CONSULTANTS:	W. A. Harrison (415) 497-4224	Stanford University
	F. A. Hummel (814) 865-4141	Penn State University
	R. G. Middleton (215) 299-1000	Philadelphia Academy of Natural Sciences

TABLE OF CONTENTS

TASK		PAGE
1.0	INTRODUCTION AND SUMMARY	pg. 1-5
1.0	SYNTHESIS	pg. 9
	1.1 Zinc Germanate ($2ZnO \cdot GeO_2$)	pg. 9
	Process Development	pg. 9
	Property Characterization	pg. 9
	Strontium Aluminate ($SrO \cdot 2Al_2O_3$)	pg. 9
	Process Development	pg. 9
	Property Characterization	pg. 9
	1.2 Niobium-Tantalum Oxide System	pg. 10
	Process Development	pg. 10
	Hafnium-Titanate Solid Solutions	pg. 13
	Process Development	pg. 13
	Property Characterization	pg. 13
	1.3 Germania Substitutions in Pollucite ($Cs_2O \cdot Al_2O_3 \cdot 4SiO_2$)	pg. 13
	Process Development	pg. 13
	Property Characterization	pg. 14
	Mullite	pg. 17
	Powder Synthesis	pg. 17
	Hot Pressing	pg. 18
	Sintering Experiments	pg. 20
	Aluminum Borate $Al_{18}B_4O_{33}$	pg. 22
	Mechanical Properties	pg. 23
	Melting Point	pg. 26
	Aluminum Niobate($AlNbO_4$)	pg. 26
	Hot Pressing	pg. 26
	Sintering of $AlNbO_4$	pg. 27
	Cadmium Aluminate, $CdAl_2O_4$	pg. 31
	Optical Transmission	pg. 33
	Thermal Expansion and Microcracking Tests	pg. 38

TABLE OF CONTENTS
(cont.)

TASK		PAGE
	Aluminum Niobate, $AlNbO_4$	pg.39
	Aluminum Borate, $Al_{18}B_4O_{33}$	pg.44
	Mullite, $Al_6Si_2O_{13}$	pg.46
	1.4 Simple Oxides	pg.46
	1.5 Non Oxide Candidate	pg.46
	Beryllium Silicon Nitride	pg.46
	1.6 Silicon-Aluminum-Oxy-Nitrides	pg.48
	$Al_5Si_6O_{15}N_3$	pg.48
	The X_1 Phase	pg.49
	1.7 Ternary Sulfides	pg.51
	Synthesis of Other Ternary Sulfide Structures	pg.51
	Thermal Stability	pg.55
	Chemical Vapor Deposition	pg.56
	IR Transmission and Lattice Vibrations	pg.56
2.0	FRACTURE TOUGHNESS ENHANCEMENT	pg.64
3.0	THERMOSTRUCTURAL ANALYSIS	pg.67
4.0	MODELLING	
	OPTICAL MODELLING OF GLOBULAR INCLUSIONS	pg.71
	Summary	pg.71a
	Microwaves	pg.73
	Light and IR	pg.74
5.0	CONTINUING SEARCH FOR IMPROVED MATERIALS	pg.77
	I. Review of Progress to Date	pg.77a
	II. Better Candidates	pg.79
	III. Low Thermal Expansion Oxides	pg.80
	IV. Nitrides as Stabilizers	pg.87

TABLE OF CONTENTS
(cont.)

TASK		PAGE
V.	Other Tetrahedral Units	pg.90
VI.	Stabilization of Other Tetrahedral Units	pg.93
VII.	Stabilization of Octrahedral Units	pg.94
VIII.	Ternary Oxides	pg.95
IX.	Summary of Recommended Materials	pg.96
REFERENCES		pg.97,98

LIST OF FIGURES

FIGURE		PAGE
1	Lattice parameters, a_0, and x-ray derived mass densities, ρ_x, for $CsAlGe_{(2-x)}Si_{(x)}O_6$, (where $0 \leq x \leq 2$)	pg.15
2	Thermal expansion and IR transmittance cut-off versus M/O $Cs_2O \cdot Al_2O_3 \cdot 4GeO_2$ pollucite solid solution	pg.16
3	Mullite sintered at 1780°C. Notice presence of a melt. Polished section, 750X.	pg.21
4	Aluminum Borate (1-5-1) hot pressed at 1500°C. Thermal etch, 300X.	pg.24
5	Aluminum Borate (1-5-2) hot pressed at 1500°C. Thermal etch, 300X.	pg.25
6	Hot-pressed aluminum niobate thermally etched specimen, SEM 16000X.	pg.28
7	Grain structure of aluminum niobate sintered at 1450°C to 98% theoretical density. Etched section, 1500X.	pg.30
8	Aluminum borate 1-5-1 hot pressed annealed t=1.15 mm.	pg.34
9	Aluminum niobate hot pressed 2-4-1 annealed (white) t=1.01 mm.	pg.35
10	Mullite hot pressed 1-7-5 annealed t=.69 mm.	pg.36
11	Mullite 1-5-2-S sintered at 1780°C t=0.74 mm.	pg.37
12	Dilatometric thermal expansion-contraction of $AlNbO_4$.	pg.40
13	Dilatometric thermal expansion-contraction of $AlNbO_4$.	pg.41
14	XRD (Guinier-Lenne camera) thermal expansion of a, b and c axes of $AlNbO_4$ and dilatometric thermal expansion of $AlNbO_4$.	pg.43

LIST OF FIGURES
(cont.)

15	Dilatometric thermal expansion-contraction of single-phase $Al_{13}B_4O_{33}$. α -25°-1000°C = 4.51×10^{-6}°C^{-1}.	pg.45
16	Dilatometric thermal expansion-contraction of single-phase $Al_6Si_2O_{13}$. α 25°-1000°C = 4.95×10^{-6}°C^{-1}.	pg.47
17	CaL_2S_4 hot pressed re-fired in H_2S 1 mm slab.	pg.57
18	Powder IR spectrum of $SrTm_2S_4$ with the $CaFe_2O_4$ structure.	pg.58
19	Powder IR spectrum of $MgEr_2S_4$ with the MnY_2S_4 structure.	pg.59
20	Powder IR spectrum of $MgHo_2S_4$ with the MnY_2S_4 structure.	pg.60
21	Raman spectrum of $SrTm_2S_4$ with the $CaFe_2O_4$ structure.	pg.62
22	Raman spectrum of $MgEr_2S_4$ with the MnY_2S_4 structure.	pg.63
23	Predicted temperature gradients using the 3-D THT program with temperature-dependent input thermal properties.	pg.69
24	Predicted thermal stresses based on a finite-element analysis of the thermal loads shown in figure 23.	pg.70

LIST OF TABLES

TABLE		PAGE
1	Summary-Synthesis-3rd Quarter	Pg.2,3,4
2	Major Candidates for Phase II	pg.6,7
3	d-spacings calculated for monoclinic $SrO \cdot 2Al_2O_3$ based on literature values of lattice parameters - a partial listing	pg.11
4	Experimental x-ray diffraction data compared with data calculated for $SrO \cdot Al_2O_3$ and $SrO \cdot 6Al_2O_3$	pg.12
5	Results of hot pressing experiments with mullite powders	pg.19
6	Microhardness of mullite	pg.20
7	Hot-pressed specimen characteristics $Al_{18}B_4O_{33}$	pg.22
8	Hot-pressing of aluminum niobate	pg.27
9	Sintering of $AlNbO_4$	pg.29
10	Synthesis of compounds with the Th_3P_4 structure	pg.52
11	Synthesis of other ternary sulfides	pg.53,54
12	Toughening systems	pg.65,66
13	Reference materials for comparative thermal shock tests	pg.68
14	Calculation for f(kd)	pg.76
15	Properties of Some Candidate Materials	pg.78
16	Octahedral and Tetrahedral Metal-Oxygen Distances in Oxide Crystals, n=4,6	pg.81,82

TABLE		PAGE
17	Metal-oxygen Distances for n=5,8	pg.83
18	Thermal Expansion Data at 1000°K for Metal-Oxide Coordination Groups	pg.84
19	Metal-nitrogen Distances and Thermal Expansion Coefficients at 1000°K.	pg.88
20	Metal-Carbon Distances and Thermal Expansion Coefficients at 1000°K	pg.89
21	Useful Binary Oxides and Nitrides	pg.91

PRECEDING PAGE BLANK-NOT FILMED

INTRODUCTION AND SUMMARY

The objective of this study is to identify and develop advanced materials suitable for electro-optical/electro-magnetic (EO/EM) windows, IR dome and radomes capable of meeting mission requirements anticipated for the 1990 decade and beyond.

This contract is a follow-on to an earlier study, Advanced Optical Ceramics - Phase "O", ONR Contract No. N00014-77-C-0649, Reference 1.

This report summarizes the work performed during the period 1 December 1978 through February 1979 on the contract. The report is organized in terms of the tasks described in the Statement of Work contained in Reference 1. The major emphasis during this reporting period has been on Task 1.0 - Synthesis, with effort continuing on Task 2.0 - Fracture Toughness Enhancement, Task 4.0 - Optical Modelling and on Task 5.0 - Continued Search for Improved Candidates.

During the third reporting period experimental work was directed at synthesis and characterization of the candidate window materials (Task 1.0). Synthesis was initiated and continued as indicated on Table 1.

The toughness enhancement study (Task 2.0) and the optical modelling (Task 4.0) continue to indicate the feasibility of toughening of optical materials. Refinements in the scattering model provided a quantitative relationship between the second phase toughener particle size - index of refraction requirement. In conjunction with known equilibria data, identification was made of the most feasible toughened systems for windows and enclosures. The most interesting candidates in this category are

(a) cubic stabilized ZrO_2/ unstabilized ZrO_2

(b) (Al_2O_3-Cr_2O_3) solid solution/unstabilized ZrO_2

because in both of these cases the index of refraction of the second phase particle is anticipated to match closely that of the matrix.

A systematic evaluation of potential new candidates (Task 5.0) was made and a theory for prediction of low coefficient of thermal expansion crystals was developed. This study identified, among others, the β' sialon ceramics as an important category.

TABLE 1

SUMMARY - SYNTHESIS - 3RD QUARTER

TASK NO.	CANDIDATE	REMARKS	MEASURED DATA
1.1	$2ZnO \cdot GeO_2$	Sintered 20.3 x 3.8 x 1.9 cm billet to 91% density. Will be press forged.	CTE = 2.63 x 10^{-6}/°C (25-1000C)
	$SrO \cdot 2Al_2O_3$	Sintered 92% dense specimen. Did not achieve Stoichiometric compound.	
1.2	$2Nb_2O_5 \cdot Ta_2O_5$	Attempts at hot pressed specimens were unsuccessful due to multiple fractures.	
	$.65(HfO_2) \cdot .35(TiO_2)$	Hot pressed samples prepared from oxide powders as well as from alkoxide precursor. Specimens off stoichiometry.	98.7% dense specimen KHN_{100}=1243 kg/mm^2
1.3	$Cs_2O \cdot Al_2O_3 \cdot 4(Si_xGe_{1-x})O_2$	Ge substitutions of the Si were successful. CTE increases and IR cut off increases with increasing Ge content.	Pollucite (all Si) • CTE=2.8 x 10^{-6}/°C • IR Cut off -4.8 um • CTE=7.2 x 10^{-6}/°C • IR Cut off - 5.0 um with 50% Si replaced by Ge
	$3Al_2O_3 \cdot 2\ SiO_2$	Powder prepared by reaction of aluminum propoxide and Si Cl_4 was successfully consolidated by both hot pressing (near theoretical density) and sintering.	

TABLE 1

SUMMARY - SYNTHESIS - 3RD QUARTER (Cont.)

TASK NO.	CANDIDATE	REMARKS	MEASURED DATA
1.3	$3Al_2O_3 \cdot 2\ GeO_2$	Sintered 20.3 x 3.8 x 1.9 cm billet to 82% density will be press forged.	• CTE = 5.38 x $10^{-6}/^oC$ (25-1000)
	$Al_{18}B_4O_{33}$	Hot pressed samples near 100% density.	• Flexstrenth (RT) = 2.34 M Nm^{-2} • Young's Modulus = 2.2×10^5 M Nm^{-2} • $T_{MP} > 1800$ C • CTE = 4.5 x $10^{-6}/^oC$ (25 - 1000C)
	$AlNbO_4$	Hot pressed samples prepared up to 99.5% density. Sintered samples prepared up to 98.2% density.	• Specimens microcrack on heating to 1000 C due to CTE anisotropy • CTE = 5.45 x $10^{-6}/^oC$ (25 - 1000C) for small grain (2.5 um) microcrack free specimens • IR Cut off ~ 6.2 um
	Cd Al_2O_4	Synthesis of solid unsuccessful to date.	
1.5	BeSiN /AlN Solid Solution	Heat treatment of two samples (a) 40 W/o AlN (b) 60 W/o AlN at 1800 C/30 HRS/700 Torr N_2	No phase separation detected.
1.6	$Al_5Si_6O_{15}N_3$	Attempts to discover the Beryl analogue in this system was unsuccessful.	

TABLE 1

SUMMARY - SYNTHESIS - 3RD QUARTER (Cont.)

TASK NO.	CANDIDATE	REMARKS	MEASURED DATA
1.6	$Si_2Al_3O_7N$ (X_1 Phase in the Sialon system)	Specimen in preparation.	
1.7	Additional Ternary Sulfides are in exploratory stage.	Powders synthesized in the MnY_2S_4 crystal structure family and spinal family such as $ZnAl_2S_4$.	MnY_2S_4 $T_{MP} \sim 1000\text{-}1200$ C

During the fourth quarter of the Advanced Optical Ceramics Phase I, the main effort will be on specimen preparation and characterization of the most promising candidates from which a selection will be made for further development in Phase II, the second year's effort. At the present time, (subject to new data which will be developed during the 4th quarter of the program), the leading candidates for the Phase II effort are listed in Table 2.

TABLE 2
MAJOR CANDIDATES FOR PHASE II
(Note Task number per Phase I Statement of Work)

	APPROX. λ CUT OFF um	CTE $\times 10^{-6}/^{\circ}C$	KHN Kg/mm^2	$T_{MP/D}$ $^{\circ}C$	COMMENTS
Task 1.1					
$2ZnO \cdot GeO_2$	6.5	2.6	486 (90% density)	1490	
Task 1.2					
$.65\ HfO_2 \cdot .35TiO_2$	6.5	2.3	1243 (98.7% density)	2200	May be microcracked due to high CTE anisotropy. May be limited to radar applications.
or					
$2Nb_2O_5 \cdot Ta_2O_5$	5.5	~ 0		1600	
Task 1.3					
$Cs_2O \cdot Al_2O_3 \cdot 4SiO_2$	4.5	2.8	606 (82% density)	>1700	Alternate candidate is $CsB_{12}Be_4Al_4O_{28}$ rhodizite (KHN $\sim$1000 kg/mm^2) - cubic
$3Al_2O_3 \cdot 2SiO_2$	4.8	5.6	1750	1880	
$3Al_2O_3 \cdot 2GeO_2$	5.5	5.4	1123 (94% density)	1530	
$B_4Al_{18}O_{33}$	5.0	4.5	1100	1947	
$(Al_2O_3\text{-}Cr_2O_3)$ Solid Solution	6.5	~ 7	~ 1600	~ 2000	Candidate for toughening using unstabilized ZrO_2 particulate additive; obtain index of refraction match by adjusting Al/Cr ratio.

TABLE 2 (Cont.)
MAJOR CANDIDATES FOR PHASE II
(Note Task number per Phase I Statement of Work)

	APPROX. λ CUT OFF um	CTE $\times 10^{-6}/^{\circ}C$	KHN Kg/mm	$T_{MP/D}$ $^{\circ}C$	COMMENTS
Task 1.4 (cont.) ZrO_2 (cubic Stabilized)	7	7.3	1100	2677	Candidate for toughening using unstabilized ZrO_2 particulate additive.
Task 1.5 AlN with $BeSiN_2$ additive	5.5	$\sim$6.0	$\sim$1200	1800	High thermal conductivity
Task 1.6 β' Sialon	4.5	2.4×10^{-6} (55% Al Equiv.)			Ge substitution for Si will be investigated to increase IR cut-off λ.
Task 1.7 $CaLaS_4$	18	>10	600	>1600	Cubic

TASK 1.0 SYNTHESIS

The main contributors to this section are:

Dr. R. A. Tanzilli	-	GE-RESD
Dr. J. J. Gebhardt	-	GE-RESD
Dr. C. Dulka	-	GE-RESD
H. W. Rauch, Sr.	-	GE-SD/SSL
A. Gatti -	-	GE-SD/SSL
Dr. S. Prochazka	-	GE-CRD
Dr. R. H. Arendt	-	GE-CRD
Dr. I. C. Huseby	-	GE-CRD
Dr. W. B. White	-	Penn State University
Dr. R. Burgner	-	Penn State University
Prof. F. A. Hummel	-	Penn State University

TASK 1.0

Task 1.1

1. Zinc Germanate ($2ZnO \cdot GeO_2$)

a) Process Development

Improvements in powder preparation, consolidation method, and sintering procedures have resulted in the preparation of a 91 percent dense sintered product. Specimens from scale-up firing (20.3 x 3.8 x 1.9 cm) will be subsequently press-forged to achieve final densities approaching theoretical.

b) Property Characterization

The thermal expansion coefficient of a sintered specimen (91% dense) was found to be $2.63 \times 10^{-6}/^{o}C$ over the temperature range from 25 to 1000°C. Specular reflectance data on 91% dense material verified stoichiometry. As mentioned previously, the estimated infrared transmittance cut-off for zinc germanate is 6.1 microns. Verification of this cut-off by direct specular and/or hemispherical transmittance measurements will be made on the highest density material achieved from the press-forging experiments. Also, completion of the planned physical property characterization matrix including an assessment of thermostructural performance potential of zinc germanate is planned for next quarter.

2. Strontium Aluminate ($SrO \cdot 2Al_2O_3$)

a) Process Development

The preparation of $SrO \cdot 2Al_2O_3$ was undertaken, as an alternative to the analagous $CaO \cdot 2Al_2O_3$, since it was believed to offer improved environmental stability together with a predicted low thermal expansion coefficient (similar to $CaO \cdot 2Al_2O_3$). A 92 percent dense specimen was prepared by sintering and submitted for phase identifications.

b) Property Characterization

Analysis of XRD patterns are in progress. Prediction of d-spacings based upon knowledge of the crystal structure of $SrO \cdot 2Al_2O_3$ was necessary since an ASTM card does not exist at the

present time for this intermediate phase. However, Boyko*and Wisnyi determined that $SrO \cdot 2Al_2O_3$ was isomorphous with monoclinic $CaO \cdot 2Al_2O_3$ and that its ($SrO \cdot 2Al_2O_3$) lattice parameters were: a = 13.04Å, b = 9.01Å, c = 5.55Å and $\beta = 106^{\circ}31'$ with four (4) formula weights in the unit cell. Using these parameters and the fact that $SrO \cdot 2Al_2O_3$ is isomorphous with $CaO \cdot 2Al_2O_3$ (for which x-ray diffraction intensity data is available, ASTM 23-1037), d-spacings were generated using the following monoclinic cell equation:

$$d_{(hkl)} = \frac{\sin\beta}{\sqrt{\left(\frac{h}{a}\right)^2 + \left(\frac{k}{b}\right)^2 \sin^2\beta + \left(\frac{l}{c}\right)^2 - \frac{2lh\cos\beta}{ca}}}$$

The d-values so generated are presented in Table 3. The associated relative intensities in this table are for the isomorph $CaO \cdot 2Al_2O_3$ (ASTM 23-1037).

Preliminary analyses of diffraction data indicate that the sintered compound is a two-phase mixture consisting of $SrO \cdot Al_2O_3$ and $SrO \cdot 6Al_2O_3$, as listed in Table 4. Thus, the higher than predicted thermal expansion data for the sintered compound listed below is not definitive for the $SrO \cdot 2Al_2O_3$ compound:

Temperature (°C)	Mean α (1/°C)
119	6.09×10^{-6}
507	7.68×10^{-6}
1006	9.03×10^{-6}

Task 1.2

1. Niobium-Tantalum Oxide System

a). Process Development

Research has now focussed on hot-pressing the $2Nb_2O_5 \cdot Ta_2O_5$ intermediate phase. Powder preparation techniques, previously described (i.e. copyrolysis of metallo-organic resinates) are being used to produce small-diameter precursor powders. Hot-pressed specimens, which are colored black after pressing, have been found to disintegrate during subsequent heat-treatment in air. This post-anneal treatment has been partially successful in renewing

*E.R.Boyko and L.G.Wisnyi, "The Optical Properties and Structures of $CaO \cdot 2Al_2O_3$ and $SrO \cdot 2Al_2O_3$", Acta Cryst. (1958).11,44.

TABLE 3 - d-SPACINGS CALCULATED FOR MONOCLINIC $SrO \cdot 2Al_2O_3$ BASED ON LITERATURE VALUES OF LATTICE PARAMETERS - A PARTIAL LISTING

d,A	I/I,*	hkl
7.31	2	110
6.25	6	200
4.69	6	$11\bar{1}$
4.51	55	020
4.00	2	111
3.78	2	310
3.65	20	220
3.54	100	$31\bar{1}$
3.438	2	021
3.278	6	$22\bar{1}$
3.125	30	400
2.920	20	130
2.803	25	221
2.764	25	311
2.645	60	$11\bar{2}$
2.568	15	420
2.501	6	$31\bar{2}$
2.491	6	131
2.463	16	$51\bar{1}$
2.437	6	330
2.389	16	$40\bar{2}$
2.253	2	040
2.230	6	202
2.119	2	240,421
2.110	2	$42\bar{2}$,$51\bar{2}$
2.084	16	600,331
.	.	.
.	.	.
.	.	.
.	.	.
.	.	.
.	.	.

*Relative intensities are actually for isomorph $CaO \cdot 2Al_2O_3$, ASTM 23-1037

TABLE 4 - EXPERIMENTAL X-RAY DIFFRACTION DATA COMPARED WITH DATA CALCULATED FOR $SrO \cdot Al_2O_3$ and $SrO \cdot 6Al_2O_3$

DIFFRACTOMETER DATA		POWDER CAMERA DATA		$SrO \cdot Al_2O_3$ (a)			$SrO \cdot 6Al_2O_3$ (b)		
d,A	I	d,A	I	d/A	I (c)	hkl	d/A	I (d)	hkl
11.1	7						11.00	70	002
5.57	12	5.6	mw				5.50	30	004
4.42	38	4.4	s	4.42	45	100	4.42	10	102
3.91	24	3.92	m	3.92	10	101	4.03	10	103
3.65	8	3.60	vvw				3.66	10	006
3.03	100	3.05	vs	3.06	100	102			
2.79	15	2.80	m				2.78	50	110
2.66	20	2.66	ms				2.63	70	107
2.55	38	2.55	ms	2.55	40	110			
2.50	12	2.51	vw				2.48	30	114
2.44	13	2.44	vw	2.44	4	111	2.41	30	200
2.38	23	2.38	mw	2.38	2	103			
2.21	12	2.21	w	2.21	12	200	2.22	30	116
2.18	13	2.18	mw	2.29	25	112			
2.13	14	2.12	w	2.12		004			
2.09	7	2.09	w				2.11	30	205
2.02	10	2.01	m				1.96	50	118
1.97	10	1.96	ms	1.96	20	202			
1.89	9	1.90	mw	1.91	12	104	1.91	30	207
.		.			.			.	
.		.			.			.	
.		PLUS 32			.			.	
.		ADDITIONAL			.			.	
.		LINES			.			.	
.			.		.			.	
.			.		.			.	
.			.		.			.	
.			.		.			.	

Notes: w - weak, m = medium, s = strong, v = very

(a) d-values were calculated using hexagonal unit cell dimensions given by Wyckoff: a = 5.10A, c = 8.49A

(b) d-values were calculated using hexagonal unit cell dimensions given by Wyckoff: a = 5.568A, c = 21.99A

(c) Intensity values presented are for isomorph $BaO \cdot Al_2O_3$ from ASTM data

(d) Intensity values presented are for isomorph β-alumina from ASTM data

the original white color (presumably due to replacing deficient oxygen), however, the disentegration of specimens remains as a problem (probably the result of the high thermal expansion anisotropy of $2Nb_2O_5 \cdot Ta_2O_5$ and too large a grain-size during hot-pressing). Better control of grain-size during hot-pressing is currently being sought.

2. Hafnium-Titanate Solid Solutions

a) Process Development

Research during this quarter has focussed on hot-pressing sintered hafniun titanate (prepared from elemental powders), and also, directly hot-pressing alkoxide-prepared powders.

b) Property Characterization

Microhardness measurements on hot-pressed specimens has produced the following:

Hot Pressed(Elemental Powders): $KHN_{100} = 1243 kg/_{mm}2$ (98.7% dense)

Hot Pressed(Alkoxide): $KHN_{100} = 1179 kg/_{mm}2$

Stoichiometry continues to be a problem with current consolidation procedures. Future processing research will focus on the 35 m/o $Ti\ O_2$ solid solution which is predicted to have an expansion coefficient of $2.3 \times 10^{-6}/^{o}C$ when prepared in a microcrack-free condition. As mentioned previously, the infrared transmittance cut-off of this phase has been deduced from specular reflectance data to be approximately 6 5 microns.

Task 1.3

1. Germania Substitutions in Pollucite ($Cs_2O \cdot Al_2O_3 \cdot 4SiO_2$)

a) Process Development

The following Ge substitutions were made in pollucite:

(1) $Cs_2O \cdot Al_2O_3 \cdot 4GeO_2$

(2) $Cs_2O \cdot Al_2O_3 \cdot 4(Si_{0.5}, Ge_{0.5})O_2$

(3) $Cs_2O \cdot Al_2O_3 \cdot 4(Si_{0.75}, Ge_{0.25})O_2$

and sintered using procedures described earlier. In addition, specimens of natural pollucite and hot-pressed synthetic pollucite were obtained for comparative measurements of end-member properties.

b) Property Characterization

Analyses of x-ray diffraction lattice parameter data, summarized in Figure 1 and tabulated below, indicate that complete solubility exists between $Cs_2O \cdot Al_2O_3 \cdot 4GeO_2$ and $Cs_2O \cdot Al_2O_3 \cdot 4SiO_2$.

Materials	a_0, A	x, g/cm^3
$CsAlGe_2O_6$	13.853	4.008
$CsAlGeSiO_6$	13.758	3.638
$CsAlSi_2O_6$	13.655	3.256
Natural Pollucite	13.670	3.245

Thermal expansion coefficient data on the various solid-solutions also exhibit a linear relationship as a function of germania substitution, however, deduced infrared cut-off data show relative insensitivity to germania contents below fifty (50) percent. These data are graphically illustrated in Figure 2.

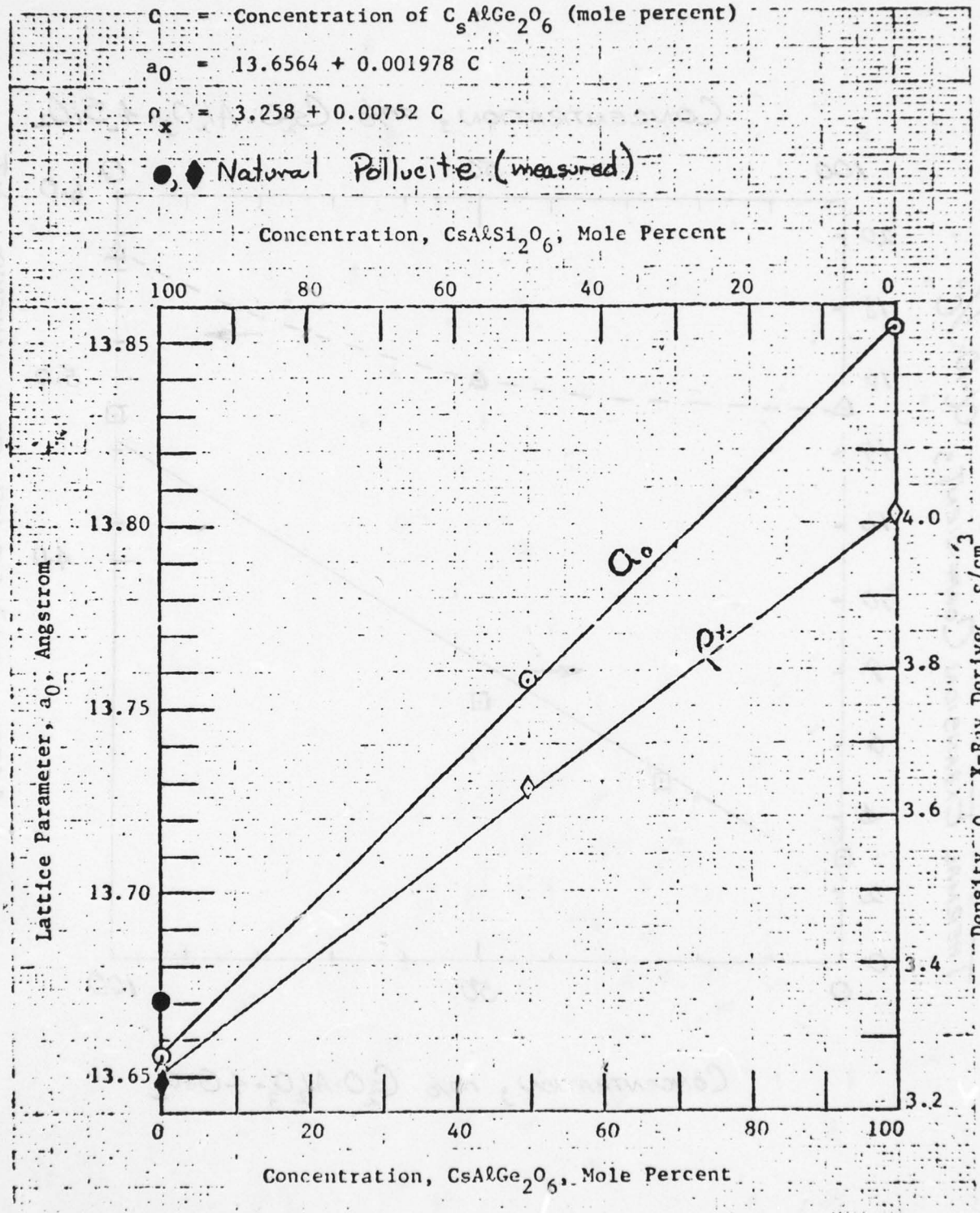


Figure 1. Lattice Parameters, a_0, and X-Ray Derived Mass Densities, ρ_x, for $CsAlGe_{(2-x)}Si_{(x)}O_6$, (where $0 \leq x \leq 2$)

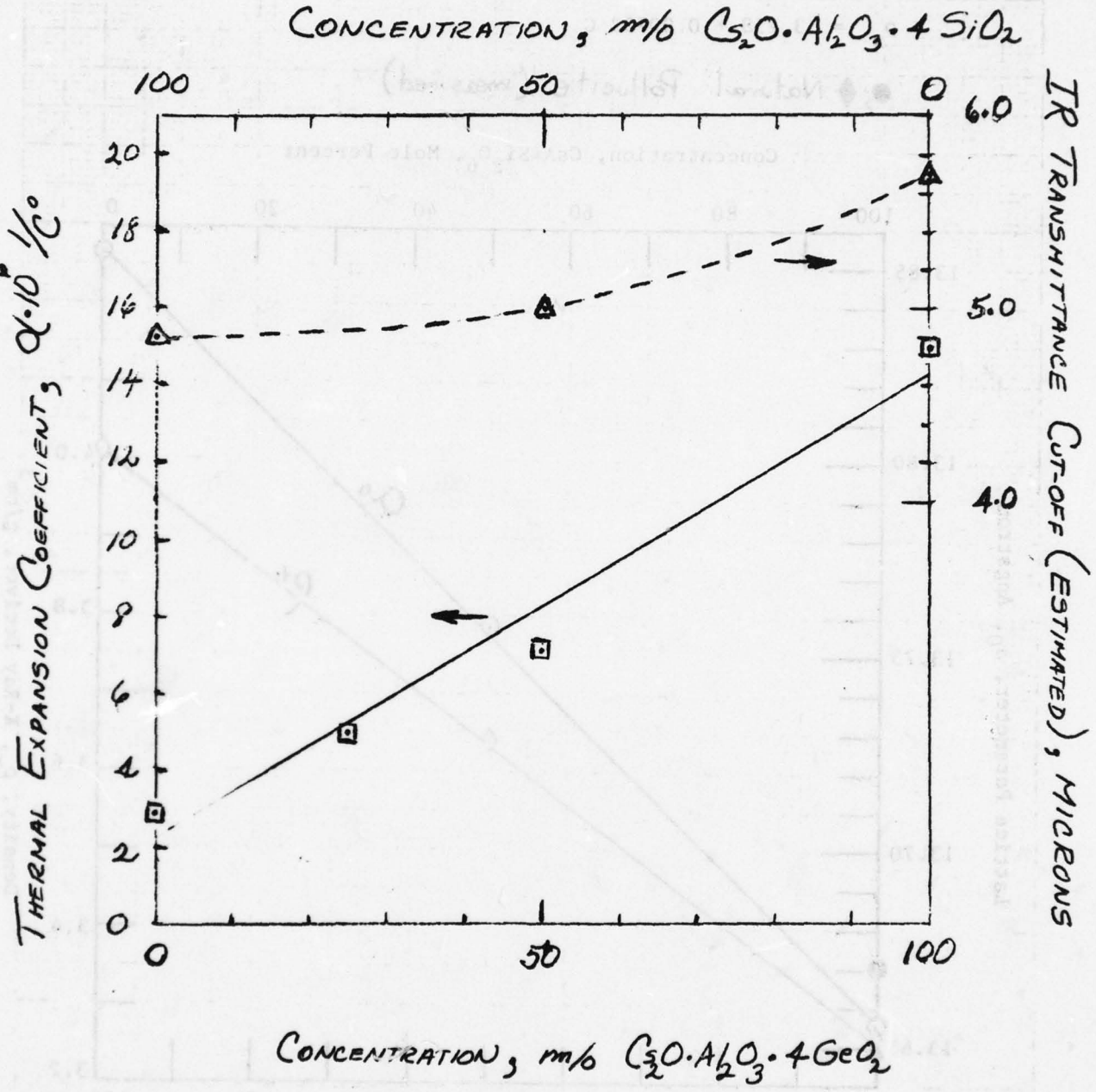


FIGURE 2. THERMAL EXPANSION AND IR TRANSMITTANCE CUT-OFF VERSUS M/O $Cs_2O \cdot Al_2O_3 \cdot 4GeO_2$ IN POLLUCITE SOLID SOLUTION.

2. Mullite

a) Powder Synthesis

Mullite prepared by synthesis from aluminum propoxide and silicon chloride was successfully consolidated both by hot pressing and sintering; this preparation technique was further developed. Work with "mullite" powder procured from HTM company and prepared by combustion of alkoxides was temporarily discontinued. The synthesis as described in the previous report (2nd quarterly R and D status report) was used to prepare several batches of amorphous powder near the $3Al_2O_3 \cdot 2SiO_2$ composition. The reproducibility seems satisfactory provided that every batch of aluminum isopropoxide is freshly distilled and its alumina content is analytically determined after that. The addition of $SiCl_4$ is then based on the actual Al_2O_3 content in aluminum isopropoxide determined gravimetrically.

The reaction of $Al(OC_3H_7)_3 + SiCl_4$ proceeds in three steps:

1. Complex formation on mixing of the two components. The complex according to cryoscopic determination in CCl_4 probably has a composition near:

$$6Al(OC_3H_7)_3 \cdot 2SiCl_4$$

This compex is a liquid at R.T. and is a relatively stable con pound judging from the large heat of reaction.

2. Heating to 165°C at 1 atm this compound starts to split off isopropylether $(C_3H_7)_2O$, and once initiated this reaction will proceed even when the temperature is decreased to as low at 105°C, however at a reduced rate. The viscosity of the reactants gradually increases.

3. If the temperature is held near 120°C isopropylchloride is given off along with the ether as the reaction progresses, a white solid product results.

4. During the final pyrolysis of this product unidentified hydrocarbons are given off along with HCl. The product of calcination is milled and calcined at 1100°C for 3 hrs. to remove traces of carbon. At this point diffuse lines of mullite can be detected by XRD. Detailed characterization of these powders requires substantially more investigation which has been planned.

b) Hot Pressing

Several specimens were hot pressed in carbon dies between 1400-1550°C and 42 MPa in vacuum. The results (Table 5) show that about 1500°C is needed to obtain densities close to theoretical (3.17 g/cc for 3.2 mullite). It was observed that unless the calcination temperature of the starting powders was such that weak diffractions of mullite could be detected by XRD the pressings would come out deep black. The coloration could be sometimes annealed out at 1400°C in about 20 hrs., however some specimens failed to respond to the annealing. It is believed that this coloration is brought about by traces of carbon. A specimen has been submitted for carbon analysis. Pressings from powders calcined at higher temperature (≥1100°C) are grey and turn white after a 1300-1350°C/20 hrs. anneal in air.

Another observation relates to lattice parameters. A substantial difference in the value of a_o has been detected in three hot pressed specimens. The origin of this variation will be investigated, it may be related to variations in the Al/Si ratio.

TABLE 5 : Results of Hot Pressing Experiments with Mullite Powders

Exp. Code Number	Hot Pressing Temp/time °C	min	Specimen Density g/cc	%	Lattice Constant a A	Remark
1-2	1400	15	2.91	91.8	---	---
1-3-1	1450	15	2.81	88.9	7.585 ±.004	Open porosity
1-5-1	1550	30	3.07	96.8	---	
1-5-2	1550	40	3.16	99.6	7.551 ±.002	Isolated Grains of Al_2O_3 by opt. mic.
1-7-1	1550	10	3.11	98.1	---	
1-7-5	1550	40	3.16	99.6	7.543 ±.002	
1-10-1	1550	40	3.17	100	---	α-Al_2O_3 by XRD

Specimen 1-7-5 (Table 5) was characterized metallographically. In agreement with the density obtained by liquid displacement, it was entirely pore free. The grain structure could not be revealed by etching and further work is needed. Isolated large grains typically 5-6 microns could be resolved. Microhardness determined by Knoop indentation is given in Table 6.

c) Sintering Experiments

Sintering experiments with mullite powders were initiated. The results show that nearly pore-free specimens can be obtained by firing in oxygen at 1750°-1790°C. Metallography and XRD analysis of the sintered samples revealed that the applied sintering conditions resulted in an increase of lattice constant (a 7.556 Å compared to 7.543 Å for the same powder hot pressed at 1550°C). At the same time a second phase appeared at triple points, which, according to the phase diagram, is expected to be a SiO_2-40% Al_2O_3 glass (Fig. 3). Because of the high SiO_2 content this phase is etched readily by dilute HF.

TABLE 6: Microhardness of Mullite*

Load	100g	500g
1	1510	1150
2	1460	1060
3	1460	1160
4	1420	1180
5	1420	1120
Average	1455	1135

*Specimen 1-7-5, Hot-Pressed, Density 3.16 g/cc.

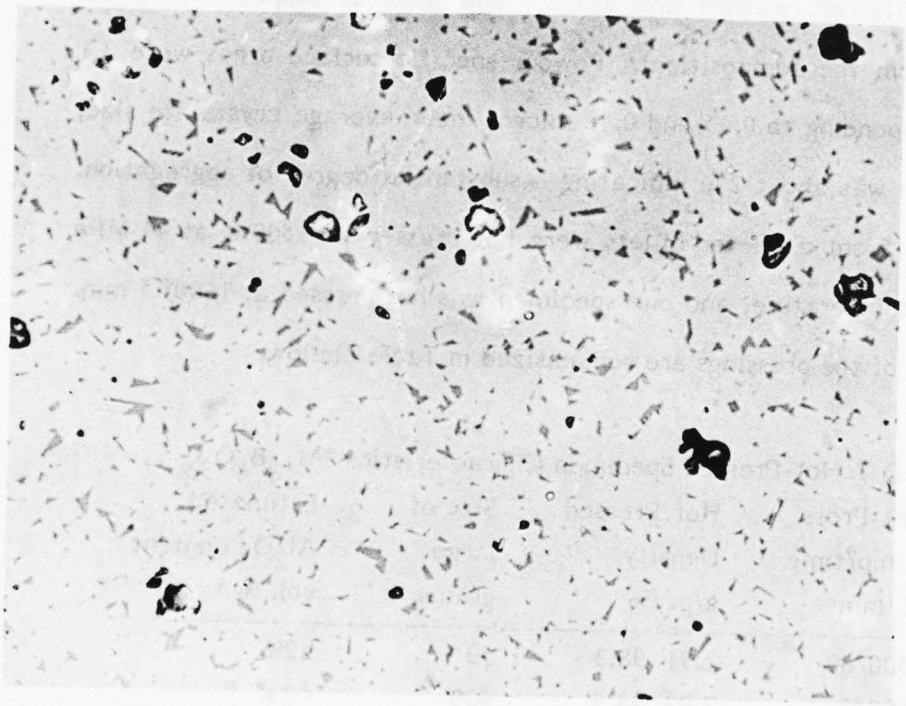


Fig. 3: Mullite Sintered at 1780°C. Notice presence of a melt. Polished Section, 750X.

3. Aluminum Borate $Al_{18}B_4O_{33}$

Two batches of $Al_{18}B_4O_{33}$ were prepared from $Al(OH)_3$ and H_3BO_3 according to the procedure described in previous report (Second Quarterly R and D Status Report). Both preparations (code no. 1-5, 1-6) were made by calcination for 24 hours at 1150°C. The test for presence of unreacted alumina by XRD (α-Alumina (113) peak) was negative. The powders were vibratory milled in methanol 10 hours by alumina balls, filtered, washed and dried. (Methanol is supposed to leach unreacted B_2O_3 from the composition). Powder specific surface areas were 3.1 and 4.2 m^2/g corresponding to 0.65 and 0.48 micron mean average crystallite size. Actual particle size was about 2 μ indicating a substantial degree of aggregation. Using this material 5 cm diameter billets were hot pressed at 1500°C at 41 MPa with 1 hr. hold at temperature, and one specimen was hot pressed at 1600° 5 min. The characteristics of the pressings are summarized in Table 7 below.

TABLE 7 Hot-Pressed Specimen Characteristics, $Al_{18}B_4O_{33}$

Code No.	Hot-Press Temp/time °C/min	Hot-Pressed Density g/cc/%	Size of large grains, μ	Estimated Al_2O_3 content vol. % *
1-5-1	1500/60	2.91 98.3	50	<2%
1-5-2	1600/5	2.93 98.9	300	<2%
1-6-1	1500/60	2.96 100	30	~3%
1-6-2	1500/60	2.97 100+	n.d.	n.d.

*Alumina was estimated by XRD

Specimen 1-5-1 was cracked after hot-pressing obviously due to adherence of the pressing to the carbon pistons and the thermal expansion mismatch between carbon and the aluminum borate. The cracking was eliminated in the following runs by using graphite foil spacers.

The grain morphologies of specimens 1-5-1 and 1-5-2 are shown in Fig. 4 and 2, which are micrographs of sections thermally etched 1 hour at 1210°C. Both show large prismatic grains growing out of a fine matrix. The matrix grain size cannot be resolved in the photographs due to overetching. It is about 1 and 3 microns for the two specimens respectively. Similar microstructures are believed to enhance fracture toughness.

In some grains, particularly in Fig. 5, faceting of some of the grain sections is clearly observed. This is usually associated with crystal growth from a liquid and consequently one suspects the presence of a melt during hot pressing, which would be, most probably, the B_2O_3 rich eutectic of the system. In order to estimate the volume fraction of the melt, experiments were conducted which would reveal this phase by a metallographic procedure. No successful etchout has yet been identified, however. The as-hot-pressed $Al_{18}B_4O_{33}$ is grey. The coloration can be annealed out entirely by heat treatment in air at 1300-1350° for about 3 days. Higher annealing temperature results in a density drop probably due to bloating. Specimens 1-6-1 and 1-6-2 were submitted for evaluation of mechanical properties, etc. which is in progress.

Mechanical Properties

Some mechanical values at room temperature have been obtained for samples (1-3-1) of aluminum borate made by hot-pressing at 1500°C to 98.6% of maximum density. These are:

$$\text{Flexural Strength (room temp.)} = 234 MNm^{-2}$$

$$\text{Young's Modulus} = 2.2 \times 10^5 MNm^{-2}$$



Fig. 4: Aluminum Borate (1-5-1) Hot Pressed at 1500°C. Thermal Etch, 300X.



Fig.5 : Aluminum Borate (1-5-2) Hot Pressed at 1600°C. Thermal etch, 300X.

Melting Point

The peritectic decomposition temperature of aluminum borate, $Al_{18}B_4O_{33}$, has been reported in the literature as 1450°C or 1950°C. In order to determine the maximum operating temperature of $Al_{18}B_4O_{33}$ a hot-pressed disc of the material was hermetically sealed inside of a tungsten crucible and heated by r.f. to 1900°C for 25 minutes. The crucible had been sealed in order to prevent loss of B_2O_3 by evaporation at these high temperatures. After the crucible was cut open, the sample was found to have melted. The residues were α-Al_2O_3 and some glass. Further tests at lower temperatures will be made to bracket the decomposition temperature. From tests in open crucibles at lower temperatures where no melting occurred we know that it is above 1800°C.

4. Aluminum Niobate ($AlNbO_4$)

a) Hot Pressing

Synthesis of this was carried out in two 60 g batches by the procedure described previously (Code No. 2-3 and 2-4). The only difference was a milling step introduced prior to calcination which was done at 750°C in vacuum for 16 hrs. to improve degassing. The product was a light tan powder, amorphous, with a specific surface area near 50 m^2/g.

Three 2" specimens were hot-pressed under vacuum in carbon dies lined with platinum foil. Table8 below gives the hot-pressing conditions and some characteristics of the pressings.

TABLE8 : Hot-Pressing of Aluminum Niobate

Code No.	Temp/Pressure °C/MPa	Density g/cc	%	Grain Size
2-3-1	1200°/41	4.20	96.2	n.d.
2-3-2	1200°/55	4.34	99.5	∽0.25μ
2-4-1	1200°/29	4.25	98.0	n.d.

Specimen 2-3-2 showed markings of a "healed" crack in the surface. This was attributed to the regime in which pressure was applied and to the high pressure. Therefore the load in the last run was lowered. This eliminated cracking, however it brought about a somewhat decreased density. Clearly further optimization of time temperature and pressure conditions are required to obtain theoretically dense bodies. The application of platinum spacers in a carbon die was successful in suppressing interaction with carbon.

The specimens are black. Annealing at 1100° for 24 hours is needed for a 1 mm thickness to remove the discoloration. The microstructure of specimen 2-3-2 is shown in Fig. 6 as revealed in a polished and thermally etched section by SEM. The average grain size is 0.25μ and the grain morphology is typical for normal grain growth of a single phase material (soap bubble structure). No pores can be observed.

b) Sintering of $AlNbO_4$

The objective of the sintering experiments was to prepare polycrystalline $AlNbO_4$ with different grain size and to determine the critical grain size which results in microcracking on thermal cycling due to the thermal expansion anisotropy.

Specimens were die pressed from $AlNbO_4$ powder no. 2-3. The powder was not suitable for die pressing because of the large specific surface area; the pressings had consequently very low green density, 33% of theoretical (4.36g/cc). Nevertheless the specimens could be sintered without difficulty in oxygen. The

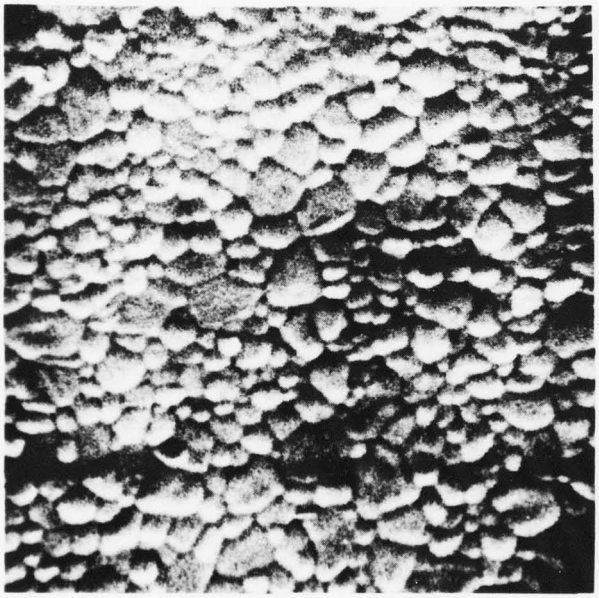


Fig. 6: Hot-Pressed Aluminum Niobate
Thermally Etched Specimen, SEM 16000X.

results in terms of sintering temperature, density, and grain size are summarized in Table 9.

TABLE 9: Sintering of $AlNbO_4$

Size No.	Sint. Temp. °C/hrs.	Density g/cc	%	Grain Size est., μ *	
1	1280°/4	3.53	81.0	0.55	SEM (fract. surface)
2	1320/3	3.99	91.5	0.95	SEM (fract. surface)
3	1370/3	4.20	96.3	n.d.	---
4	1450/16	4.28	98.2	4.8	Linear Count (section)
5	1480/16	4.28	98.0	>10μ	Est. from as-fired surface
	Hot-Pressed 1200°C	4.34	99.5	0.25	SEM

* In determining grain size by SEM average size is reported; in determination by mean linear intercept count in a section by optical microscopy a factor of 1.5 has been applied as usual.

From Table 9 it is observed that a terminal density of 98% theoretical is obtained near 1400°. Further increase in temperature does not bring about any additional reduction in porosity. It is anticipated that a substantial fraction of this residual porosity is related to microcracking. Fig. 7 shows an example of the grain structures observed in $AlNbO_4$ sintered to its terminal density. Essentially all the pores observed in this section are due to grain pull-out during specimen preparation. The loose grains are caused by microcracking. As reported in the next paragraph, thermal expansion hystersis has not been observed in hot pressed specimens and in specimen no. 1 (sintered at 1280°C). However it has been clearly detected in specimens nos. 2,3 and 4 in an increasing degree. It may be concluded therefore that polycrystalline $AlNbO_4$ with grain size 1μ and larger undergoes microcracking during a room temperature to 1000°C excursion.



Fig. 7: Grain Structure of Aluminum Niobate Sintered at 1450°C to 98% Theoretical Density. Etched Section, 1500X.

Although some improvements in grain growth control may be obtained (particularly by optimization of the starting powder properties), it is unlikely that theoretically dense $AlNbO_4$ with grain size less than 1 μ could be obtained by sintering. In other words in order to prevent microcracking in polycrystalline samples the grain size has to be substantially less than 1 μ, and this type of grain structure along with theoretical density can be obtained only by hot-pressing.

5. Cadmium Aluminate, $CdAl_2O_4$

A sample of the candidate optical ceramic material $CdAl_2O_4$ has been prepared. This material supposedly crystallizes with rhombohedral symmetry and the phenacite structure type (F. Cohn, Rev. Int. Hautes Temp. Refract. 5 (4), 277 (1968)). According to the literature this compound should be stable in the temperature regime 1073-1273K, particularly in the presence of excess CdO. There are two other compounds in this system: $CdAl_4O_7$ and $CdAl_{12}O_{19}$. Since there are no compounds richer in CdO than the candidate, reaction conditions utilizing excess CdO should yield $CdAl_2O_4$.

The sample was prepared by reaction of the appropriate oxides in a solution with molten NaCl-50 wt% KCl (mp ~931K), a technique which had previously been found to yield stoichiometric, monodispersed, small-crystallite-size oxide powders. The reaction mixture consisted of 91.97 g CdO (wt% excess), 101.58 g $Al(OH)_3$, 65.91 g NaCl and 84.09 g KCl. This mixture contained ~50 wt% chloride solvent based on a reacted composition. The components were dry mixed by tumbling overnight in a plastic jar. The uniformly appearing mixture was placed in a dense, covered α-Al_2O_3 crucible and reacted at 1073-1093 K for one hour in an air atmosphere. The solidified, reacted cake was uniform in appearance, with evidence that a liquid phase had been present.

The reacted cake was placed in ~4 liters of distilled H_2O and the chloride salts dissolved to yield a finely dispersed, deflocculated purple powder. Flocculation and settling of this material was accomplished using an anionic organic flocculating agent; the supernatant solution was decanted for disposal. Another 4 liter of H_2O containing 200 ml glacial acetic acid was added to the soluble material. The color of the material changed from purple to very light yellow when it contacted the acetic acid solution, indicating that the purple coloration was due to CdO. The initial acid content was not sufficient to dissolve all the CdO present (although it should have been) and another 200 ml glacial acetic acid was required to accomplish the task.

The product was flocculated as before and the supernatant solution, now containing Cd^{+2}, was removed for disposal. The wash/decant procedure was repeated six additional times to yield a final residual soluble impurity level, based on a 20:1 dilution factor for each wash, of $<1 \times 10^{-6}$. The product was dried at ~473 K in Teflon labware and supplied for analysis.

Based on the glacial acetic acid requirement and product mass yield, the product is most consistent with $CdAl_{12}O_{19}$ rather than the intended $CdAl_2O_4$. Should this conclusion be substantiated, additional samples can be prepared using a modified synthetic technique. X-ray diffraction studies on a hot-pressed sample of this powder showed the structure to be that of α-Al_2O_3. Apparently almost all of the CdO disappeared during processing. A second sample is being prepared.

Optical Transmission (Task 1.3 Candidates)

Optical transmission measurements at room temperature have been made on several samples of oxide materials. The results are shown in Figs. 8-11 for the wavenumber region 1500cm^{-1} to 3100cm^{-1} (6.67 micron to 3.23 micron wavelengths). For samples of the order of 1 mm thick the total, in-line transmission was 5 to 10% in the most transparent regions. However for one mullite sample, Fig. 10 the maximum transmission was 77%. These numbers are for the net transmission with surface reflection losses present.

Let us consider the results in Fig. 10 more closely. For an average refractive index of n=1.64 the single surface reflection loss at normal incidence will be:

$$R = \left(\frac{n-1}{n+1}\right)^2 = 0.0588$$

For two surfaces the maximum transmission will be: $T = (1-R)^2 = 88.6\%$. Thus at $\bar{\nu}$ = 2400cm^{-1} the internal scattering and absorption losses correspond to an optical loss coefficient of, α, of

$$e^{-\alpha x} = 0.76/0.886 = 0.858$$

or

$$\alpha = 2.2 \text{ cm}^{-1}$$

These results are for sample 1-7-5 which, from Table 5 has a density of 99.6% of theoretical. Whether the losses are caused by the residual porosity, refractive index anisotropy, or second phase inclusions is not yet certain.

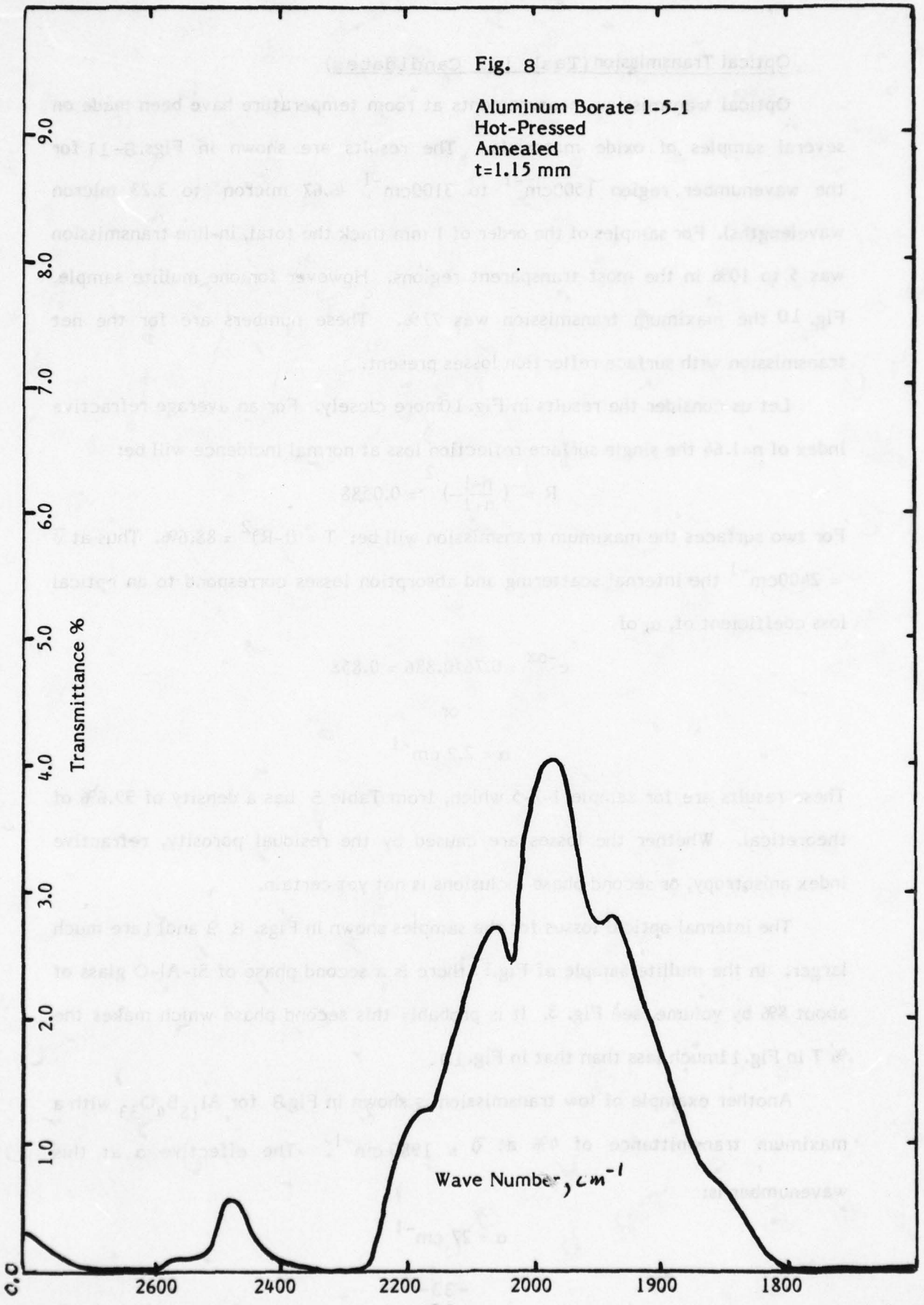
The internal optical losses for the samples shown in Figs. 8, 9 and 11 are much larger. In the mullite sample of Fig. 11 there is a second phase of Si-Al-O glass of about 8% by volume, see Fig. 3. It is probably this second phase which makes the % T in Fig. 11 much less than that in Fig. 10.

Another example of low transmission is shown in Fig. 8 for $Al_{18}B_4O_{33}$ with a maximum transmittance of 4% at $\bar{\nu}$ = 1980 cm^{-1}. The effective α at this wavenumber is:

$$\alpha = 27 \text{ cm}^{-1}$$

Fig. 8

Aluminum Borate 1-5-1
Hot-Pressed
Annealed
t=1.15 mm



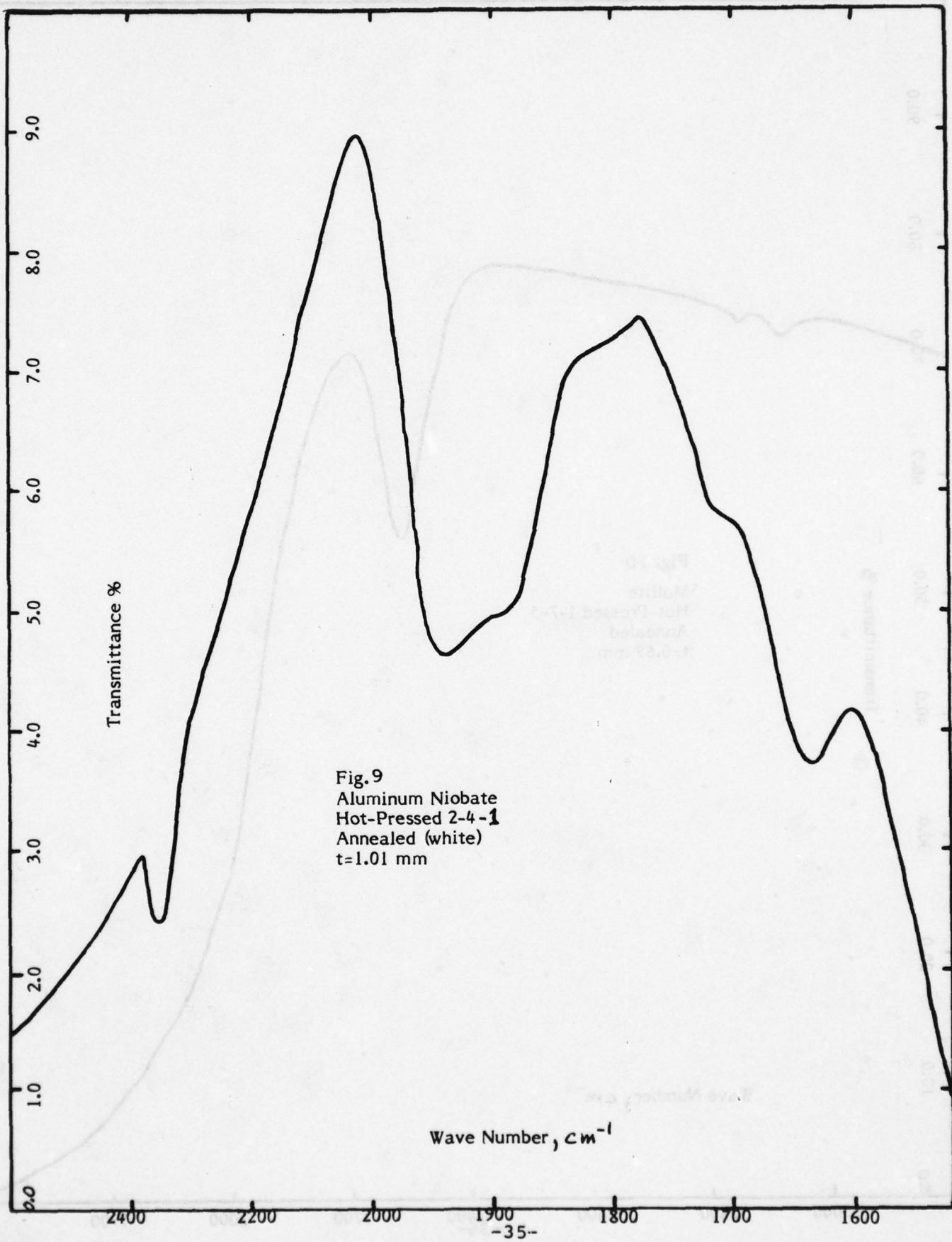


Fig. 9
Aluminum Niobate
Hot-Pressed 2-4-1
Annealed (white)
t=1.01 mm

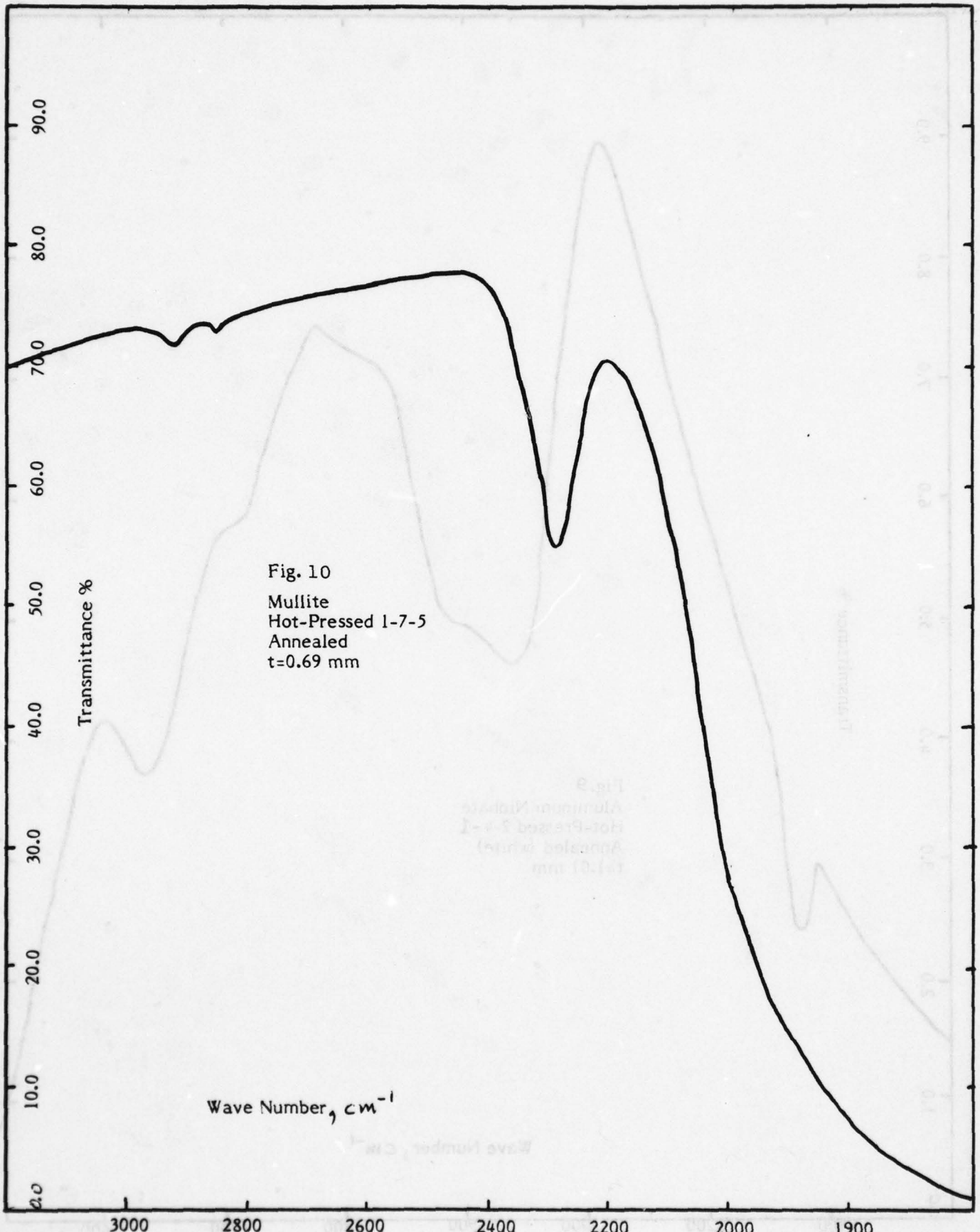
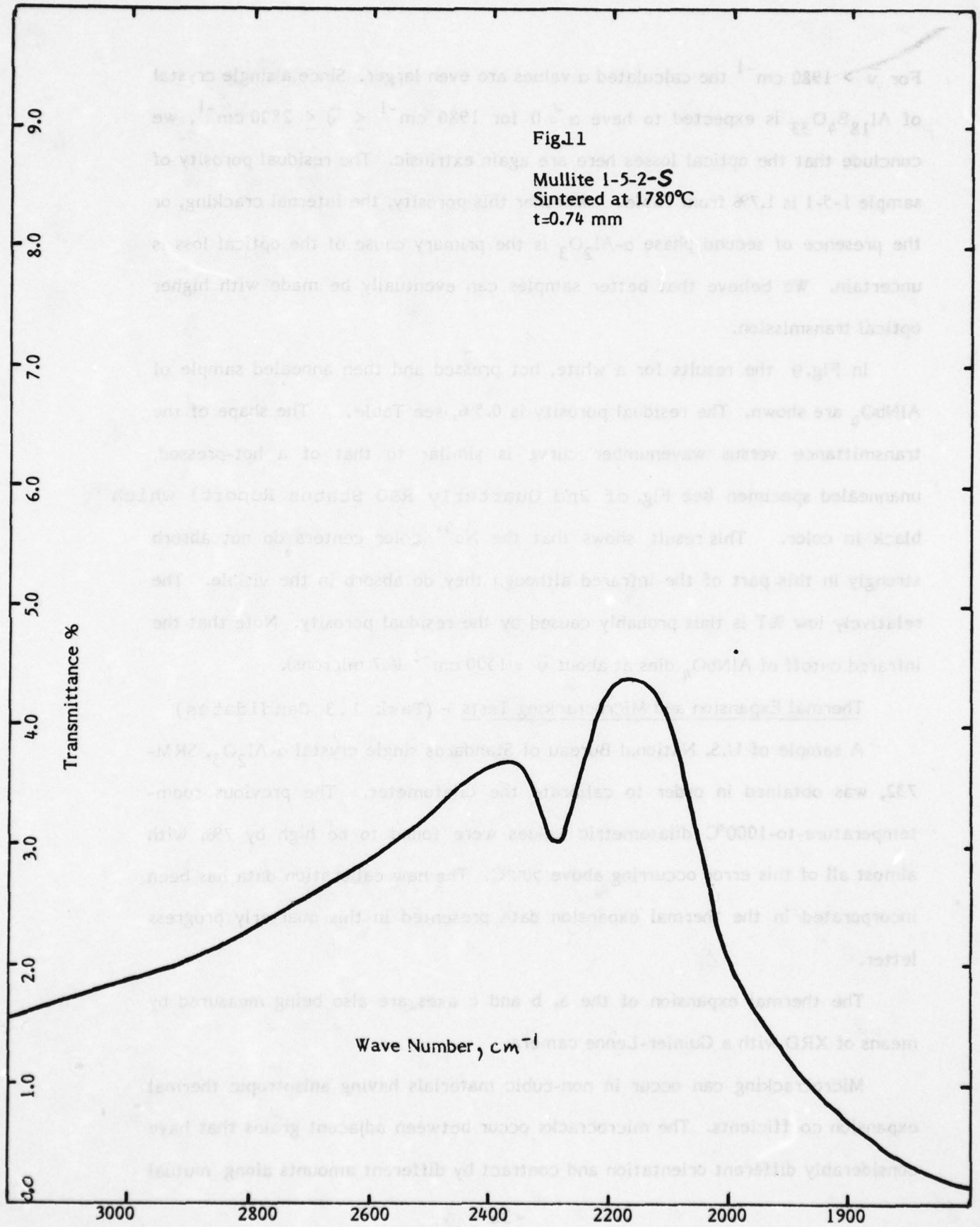


Fig. 10

Mullite
Hot-Pressed 1-7-5
Annealed
t=0.69 mm


Fig.11
Mullite 1-5-2-S
Sintered at 1780°C
t=0.74 mm
Transmittance %
9.0
8.0
7.0
6.0
5.0
4.0
3.0
2.0
1.0
0.0
3000
2800
2600
2400
2200
2000
1900
Wave Number, cm⁻¹

For $\bar{\nu} > 1980\ cm^{-1}$ the calculated α values are even larger. Since a single crystal of $Al_{18}B_4O_{33}$ is expected to have $\alpha \stackrel{\sim}{=} 0$ for $1980\ cm^{-1} \leq \bar{\nu} \leq 2800\ cm^{-1}$, we conclude that the optical losses here are again extrinsic. The residual porosity of sample 1-5-1 is 1.7% from Table. Whether this porosity, the internal cracking, or the presence of second phase α-Al_2O_3 is the primary cause of the optical loss is uncertain. We believe that better samples can eventually be made with higher optical transmission.

In Fig. 9 the results for a white, hot pressed and then annealed sample of $AlNbO_4$ are shown. The residual porosity is 0.5%, see Table. The shape of the transmittance versus wavenumber curve is similar to that of a hot-pressed, unannealed specimen (see Fig. of 2nd Quarterly R&D Status Report) which black in color. This result shows that the Nb^{4+} color centers do not absorb strongly in this part of the infrared alth ugh they do absorb in the visible. The relatively low %T is thus probably caused by the residual porosity. Note that the infrared cutoff of $AlNbO_4$ dies at about $\bar{\nu} = 1500\ cm^{-1}$ (6.7 microns).

Thermal Expansion and Microcracking Tests - (Task 1.3 Candidates)

A sample of U.S. National Bureau of Standards single crystal α-Al_2O_3, SRM-732, was obtained in order to calibrate the dilatometer. The previous room-temperature-to-1000°C dilatometric values were found to be high by 7%, with almost all of this error occurring above 500°C. The new calibration data has been incorporated in the thermal expansion data presented in this quarterly progress letter.

The thermal expansion of the a, b and c axes are also being measured by means of XRD with a Guinier-Lenne camera.

Microcracking can occur in non-cubic materials having anisotropic thermal expansion coefficients. The microcracks occur between adjacent grains that have considerably different orientation and contract by different amounts along mutual

directions. Thus, the microcracks have a diameter about as large as one grain and a crack opening displacement equal to $\Delta\alpha\Delta Td$, where $\Delta\alpha$ is the difference in thermal expansion between the two adjacent grains in the directions of the crack opening displacement, ΔT the temperature differential between the sintering temperature and the temperature in question, and d the grain diameter of the two adjacent grains. The displacements are very small, for example, with 4μm grain size $AlNbO_4$, the crack opening displacements are in the order of 0.01μm. Microcracks are expected to be scattering centers for electromagnetic radiation.

a) Aluminum Niobate, $AlNbO_4$

In the 2nd Quarterly Report it was reported that microcracking may be occurring with the $AlNbO_4$ samples. This progress letter reports additional results concerning microcracking in $AlNbO_4$.

Figs. 12 and 13 show the dilatometric thermal expansion-contraction of $AlNbO_4$ samples which were sintered at various temperatures to produce different average grain sizes. The heat treatments were used to investigate the influence of the grain size of $AlNbO_4$ on microcracking. Fig. 12 shows the thermal expansion-contraction of two samples, one containing an average grain size of ~0.55μm and the other an average grain size of 4.8μm. The expansion-contraction curve of the ~0.55μm grain size sample is normal and indicates that microcracking did not occur. The expansion-contraction curve of the 4.8μm grain size sample is vastly different and contains the following noticeable effects: (1) a large hysteresis (2) the 25°-1000°C expansion is only about half that of the fine grain sample (3) the 1000°-400°C contraction is about the same as that of the fine grain sample (4) below ~400°C the slope of the cooling curve changes dramatically and at 100°C changes sign. During cooling below 100°C the sample elongates, and at room temperature the sample continued to elongate.

The expansion-contraction of the coarse grain sample was remeasured and found to be reproducible. The above effects are due to microcracking. During the

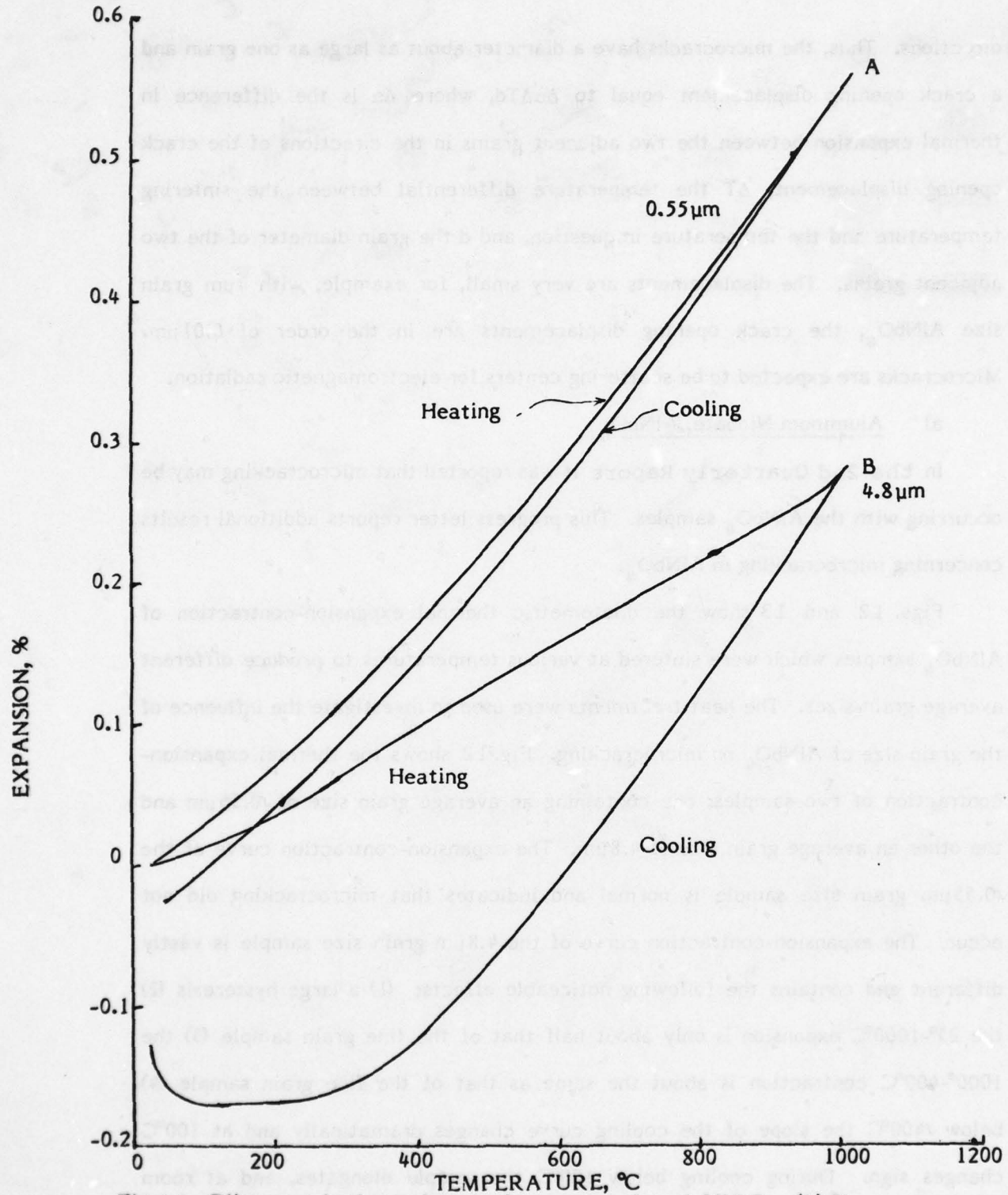


Fig. 12: Dilatometric thermal expansion-contraction of $AlNbO_4$. (A) Sintered 3 hours in air at 1280°C, average grain size = 0.55µm. (B) Sintered in oxygen at 1450°C, average grain size = 4.8µm. α-25°-1000°C (microcrack free) = 5.45×10^{-6} °C^{-1}.

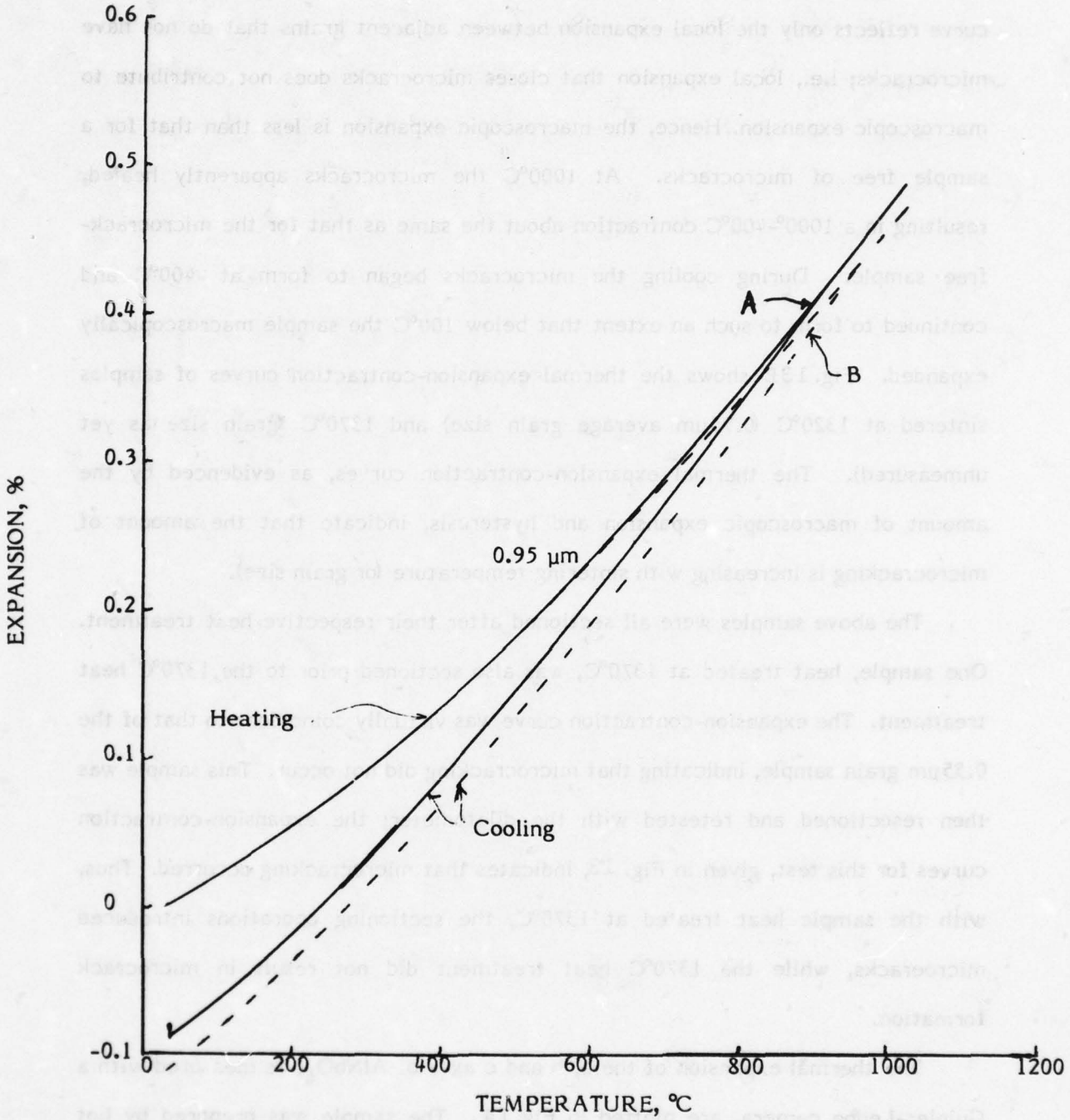


Fig. 13: Dilatometric thermal expansion-contraction of $AlNbO_4$. (A) Sintered 3 hours in air at 1320°C, average grain size = 0.95 µm. (B) Sintered 3 hours in air at 1370°C.

25°-1000°C expansion the microcracks begin to close. The 25°-1000°C expansion curve reflects only the local expansion between adjacent grains that do not have microcracks; i.e., local expansion that closes microcracks does not contribute to macroscopic expansion. Hence, the macroscopic expansion is less than that for a sample free of microcracks. At 1000°C the microcracks apparently healed, resulting in a 1000°-400°C contraction about the same as that for the microcrack-free sample. During cooling the microcracks began to form at ~400°C and continued to form to such an extent that below 100°C the sample macroscopically expanded. Fig. 13B shows the thermal expansion-contraction curves of samples sintered at 1320°C (0.95μm average grain size) and 1370°C (grain size as yet unmeasured). The thermal expansion-contraction curves, as evidenced by the amount of macroscopic expansion and hysteresis, indicate that the amount of microcracking is increasing with sintering temperature (or grain size).

The above samples were all sectioned after their respective heat treatment. One sample, heat treated at 1370°C, was also sectioned prior to the 1370°C heat treatment. The expansion-contraction curve was virtually coincident to that of the 0.55μm grain sample, indicating that microcracking did not occur. This sample was then resectioned and retested with the dilatometer; the expansion-contraction curves for this test, given in Fig. 13, indicates that microcracking occurred. Thus, with the sample heat treated at 1370°C, the sectioning operations introduced microcracks, while the 1370°C heat treatment did not result in microcrack formation.

The thermal expansion of the a, b and c axes of $AlNbO_4$, as measured with a Guinier-Lenne camera, are plotted in Fig. 14. The sample was prepared by hot pressing $AlNbO_4$ and Pt powder together in a BN coated graphite die at 1000°C for 10 minutes, with the Pt serving as an X-ray standard. The expansion measurements assume a monoclinic structure for $AlNbO_4$. The dilatometric thermal expansion is

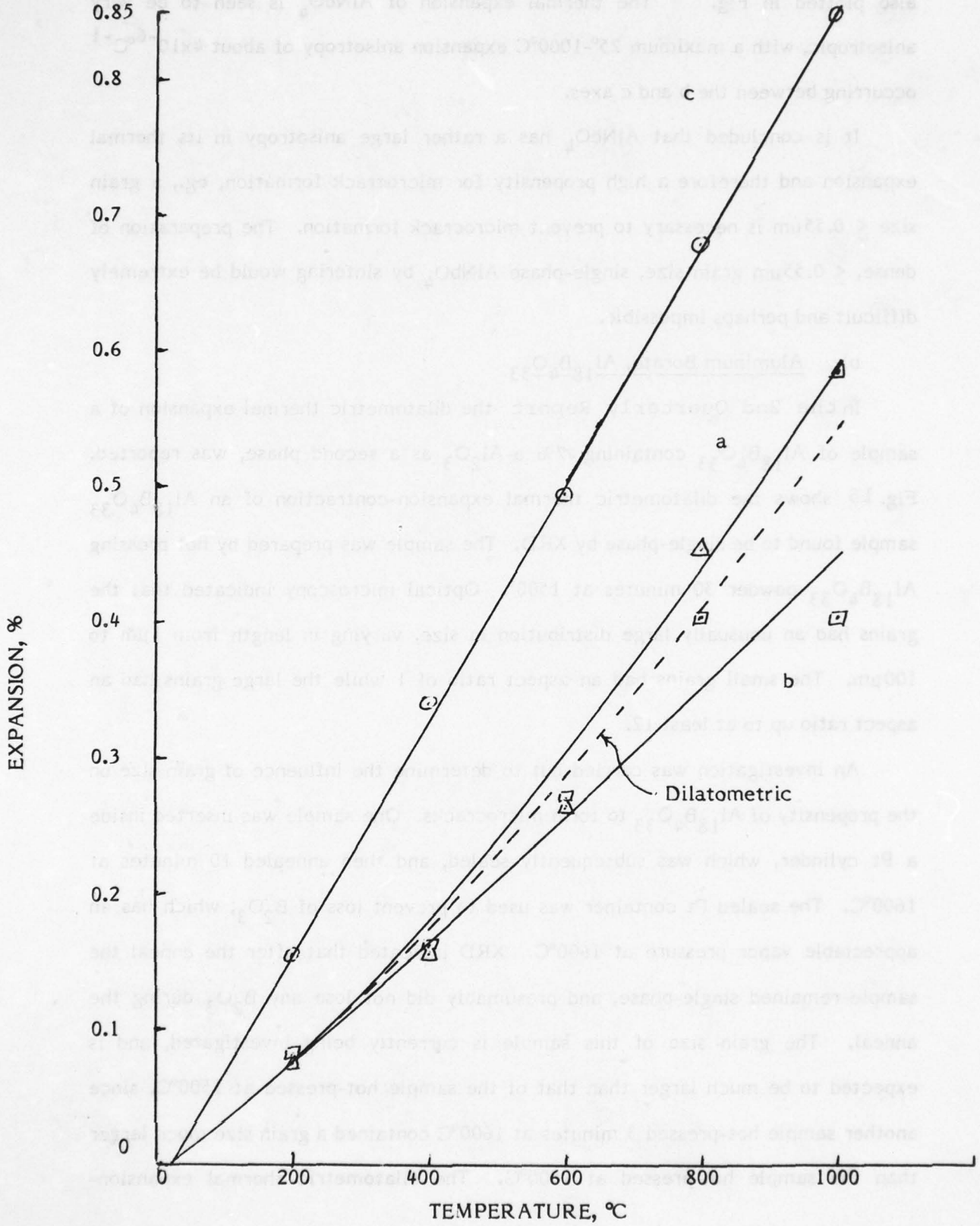


Fig. 14 XRD (Guinier-Lenne camera) thermal expansion of a, b and c axes of $AlNbO_4$ and dilatometric thermal expansion of $AlNbO_4$.

also plotted in Fig. The thermal expansion of $AlNbO_4$ is seen to be very anisotropic, with a maximum 25°-1000°C expansion anisotropy of about $4 \times 10^{-6} °C^{-1}$ occurring between the b and c axes.

It is concluded that $AlNbO_4$ has a rather large anisotropy in its thermal expansion and therefore a high propensity for microcrack formation, eg., a grain size $\leq$ 0.55μm is necessary to prevent microcrack formation. The preparation of dense, $\leq$ 0.55μm grain size, single-phase $AlNbO_4$ by sintering would be extremely difficult and perhaps impossible.

b) Aluminum Borate, $Al_{18}B_4O_{33}$

In the 2nd Quarterly Report the dilatometric thermal expansion of a sample of $Al_{18}B_4O_{33}$ containing ~7% α-Al_2O_3 as a second phase, was reported. Fig. 15 shows the dilatometric thermal expansion-contraction of an $Al_{18}B_4O_{33}$ sample found to be single-phase by XRD. The sample was prepared by hot pressing $Al_{18}B_4O_{33}$ powder 30 minutes at 1500°. Optical microscopy indicated that the grains had an unusually large distribution in size, varying in length from 1μm to 100μm. The small grains had an aspect ratio of 1 while the large grains had an aspect ratio up to at least 12.

An investigation was carried out to determine the influence of grain size on the propensity of $Al_{18}B_4O_{33}$ to form microcracks. One sample was inserted inside a Pt cylinder, which was subsequently sealed, and then annealed 10 minutes at 1600°C. The sealed Pt container was used to prevent loss of B_2O_3, which has an appreciable vapor pressure at 1600°C. XRD indicated that after the anneal the sample remained single-phase, and presumably did not lose any B_2O_3 during the anneal. The grain size of this sample is currently being investigated, and is expected to be much larger than that of the sample hot-pressed at 1500°C, since another sample hot-pressed 3 minutes at 1600°C contained a grain size much larger than the sample hot-pressed at 1500°C. The dilatometric thermal expansion-

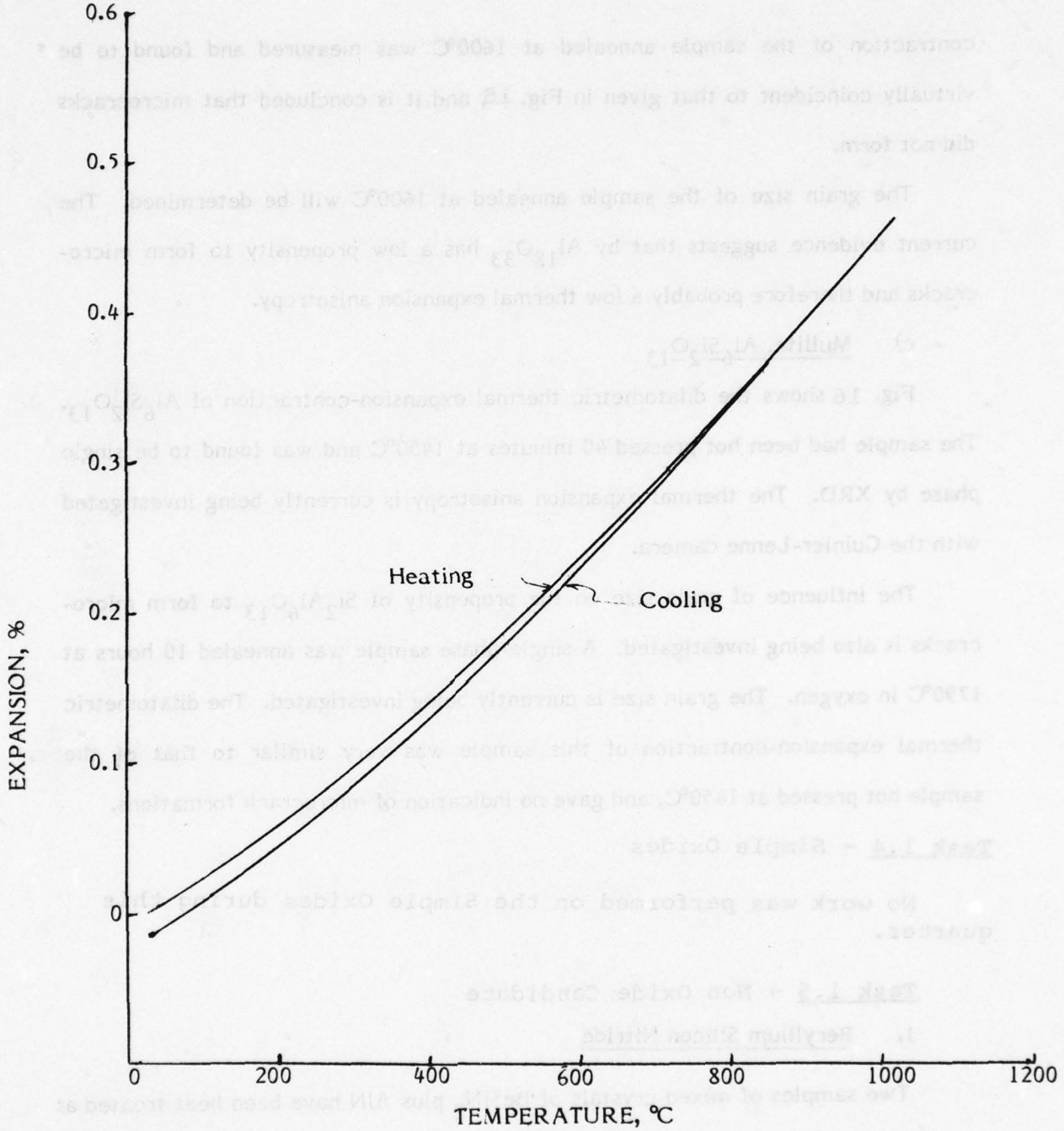


Fig. 15: Dilatometric thermal expansion-contraction of single-phase $Al_{18}B_4O_{33}$. α-25°-1000°C = 4.51×10^{-6}°C^{-1}.

contraction of the sample annealed at 1600°C was measured and found to be virtually coincident to that given in Fig. 15, and it is concluded that microcracks did not form.

The grain size of the sample annealed at 1600°C will be determined. The current evidence suggests that by $Al_{18}O_{33}$ has a low propensity to form microcracks and therefore probably a low thermal expansion anisotropy.

c) Mullite, $Al_6Si_2O_{13}$

Fig. 16 shows the dilatometric thermal expansion-contraction of $Al_6Si_2O_{13}$. The sample had been hot pressed 40 minutes at 1450°C and was found to be single phase by XRD. The thermal expansion anisotropy is currently being investigated with the Guinier-Lenne camera.

The influence of grain size on the propensity of $Si_2Al_6O_{13}$ to form microcracks is also being investigated. A single-phase sample was annealed 10 hours at 1790°C in oxygen. The grain size is currently being investigated. The dilatometric thermal expansion-contraction of this sample was very similar to that of the sample hot pressed at 1450°C, and gave no indication of microcrack formations.

Task 1.4 - Simple Oxides

No work was performed on the Simple Oxides during this quarter.

Task 1.5 - Non Oxide Candidate

1. Beryllium Silicon Nitride

Two samples of mixed crystals of $BeSiN_2$ plus AlN have been heat treated at 1800°C for thirty hours in nitrogen gas at a pressure of 700 Torr using a tungsten crucible (Run W-218) to hold the previously hot-pressed, dense samples. The samples, before heat-treatment, were single phase mixed crystals with hexagonal crystal structure, and contained 40 weight % and 60 weight % AlN respectively. After the heat treatment they were studied by X-rays in order to look for possible phase separation.

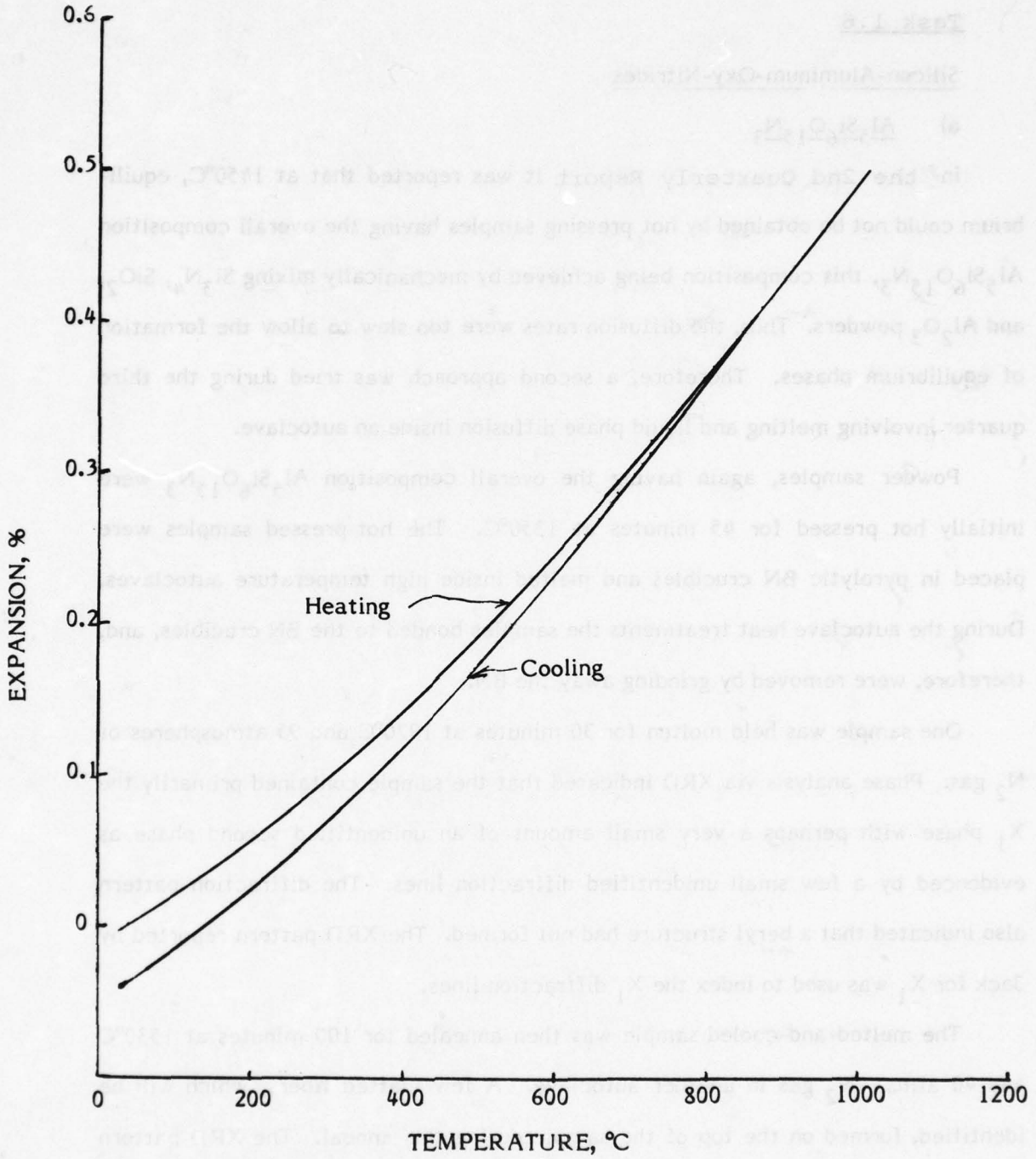


Fig.16: Dilatometric thermal expansion-contraction of single-phase $Al_6Si_2O_{13}$. α 25°-1000°C = 4.95×10^{-6} °C^{-1}.

Task 1.6

Silicon-Aluminum-Oxy-Nitrides

a) $Al_5Si_6O_{15}N_3$

In the 2nd Quarterly Report it was reported that at 1450°C, equilibrium could not be obtained by hot pressing samples having the overall composition $Al_5Si_6O_{15}N_3$, this composition being achieved by mechanically mixing Si_3N_4, SiO_2, and Al_2O_3 powders. Thus, the diffusion rates were too slow to allow the formation of equilibrium phases. Therefore, a second approach was tried during the third quarter involving melting and liquid phase diffusion inside an autoclave.

Powder samples, again having the overall composition $Al_5Si_6O_{15}N_3$ were initially hot pressed for 45 minutes at 1350°C. The hot-pressed samples were placed in pyrolytic BN crucibles and melted inside high temperature autoclaves. During the autoclave heat treatments the samples bonded to the BN crucibles, and, therefore, were removed by grinding away the BN.

One sample was held molten for 30 minutes at 1970°C and 95 atmospheres of N_2 gas. Phase analysis via XRD indicated that the sample contained primarily the X_1 phase with perhaps a very small amount of an unidentified second phase as evidenced by a few small unidentified diffraction lines. The diffraction pattern also indicated that a beryl structure had not formed. The XRD pattern reported by Jack for X_1 was used to index the X_1 diffraction lines.

The melted-and-cooled sample was then annealed for 100 minutes at 1530°C and 40 atms. N_2 gas in another autoclave. A few matted fibers, which will be identified, formed on the top of the sample during this anneal. The XRD pattern for the sample after the anneal was almost identical to that taken prior to the anneal, the only difference being that the annealing treatment resulted in slightly sharper diffraction lines.

A second hot-pressed sample was melted for 10 minutes at 1900°C and 68 atmosphere of N_2 gas. During the melting process the sample lost 0.7 wt%; this was determined by assuming that all of the sample-crucible system weight loss occurred from the sample. Optical microscopy, including one thin section, and XRD indicated that the sample contained a crystalline outer shell of X_1 surrounding an amorphous matrix. The amorphous matrix also contained isolated crystals of X_1. The sample was then sectioned, and the various sections were annealed for 2 hours at 1000°, 1200° and 1400°C, and 16 hours at 1400°C. At 1000°C the glass did not begin to devitrify and the XRD pattern was the same as that prior to the anneal. At 1200°C the glass began to devitrify and form additional X_1. After 2 hours at 1400°C the sample was found to contain X_1, and α-cristobalite, and after an additional 14 hours at 1400°C the sample contained X_1 and mullite. It is uncertain as to why the cristobalite and mullite formed, but it may be that this particular sample contained a small clump of unreacted SiO_2. In addition, the N_2, which was not high purity, may have contained an O_2 content sufficient to oxidize the outer surface of the sample and form mullite. XRD indicated that a beryl structure did not form during any of these heat treatments.

It is concluded that, at least under these conditions, a beryl structure having the composition $Al_5Si_6O_{15}N_3$ does not exist. The possible existence of such a structure had been posulated by taking $Be_3Al_2Si_6O_{18}$ and making the substitution of 3AlN for 3BeO in the structure.

b) The X_1 Phase

The exact composition of X_1 is uncertain, however, Jack's* latest reported composition, $Si_2Al_3O_7N_1$, is close to Gauckler et al's latest reported composition, $Si_{12}Al_{78}O_{39}N_8$. The complete structure is also uncertain, with Jack currently reporting X_1 to be monoclinic.

*"High Temperature Chemistry of Inorganic and Ceramic Materials" Keele University, Sept. 1976, ed. F.P.Glasser, P.E.Potter, pub. Chemical Society, Burlington House, London.

Two different thermal expansion values have been reported for X_1, $3.6 \times 10^{-6} {}^{o}C^{-1}$ by Gauckler et al and $6 \times 10^{-6} {}^{o}C^{-1}$ by Thompson et al. If the lower value is correct, the X_1 may be an interesting candidate for advanced optical windows.

Therefore, an attempt is being carried out to measure the thermal expansion of X_1. A powder mixture, having the overall composition $Si_2Al_3O_7N_1$ has been prepared by ball milling a mixture of α-Al_2O_3 and α-Si_3N_4, and SiO_2 (quartz) powders for 52 hours in a plastic jar with heptane and Al_2O_3 milling balls. Isostatic pressings were made using this powder mixture, and one of the isostatic pressings was placed in a BN boat inside an autoclave and melted for 40 minutes at 1900°C and 720-840 psi N_2. During the test the sample lost 5.7 wt%, some of which was water vapor. The XRD pattern for this sample is currently being investigated. A rod-shaped section will also be diamond cut from this sample for dilatometric thermal expansion analysis.

Task 1.7 Ternary Sulfides

Synthesis of Th_3P_4 Type Compounds

The main effort this quarter has been the synthesis of larger quantities of $CaLa_2S_4$ identified as the most likely candidate for a window material. It has proved possible to prepare 50 gram charges routinely.

Other members of the Th_3P_4 family are listed in Table10 which is a compilation of new synthesis runs during the quarter.

Synthesis of Other Ternary Sulfide Structures

New synthesis runs during the quarter are listed in Table 11. Table 10 and Table 11 are lists of new runs and supplement the list of runs given in the second quarterly report.

Most of the effort has been on compounds of the MnY_2S_4 structure type. There are two series of these: Mg(small rare earth)$_2S_4$ and Mn(small rare earth)$_2S_4$. The magnesium compounds are fairly easy to synthesize, the manganese compounds more difficult. This is seen as a lucky combination in that manganese is more likely to be plagued with mixed valence states and unwanted electronic absorption than are the magnesium compounds.

Ternary sulfides with the MnY_2S_4 type structure seem to be less stable than the compounds of the Th_3P_4 type. Some seem to melt in the range of 1000 - 1200°C and they appear to be more volatile and reactive with the ambient

Table 10

Synthesis of Compounds with the Th_3P_4 Structure

Compound	Run and Number	Starting Material	Conditions	Phases (trace unless noted)			Comments
$CaLa_2S_4$	29	Batches 8, 21, 27	3d;1070°	CaS	0	0	
	48	$CaCO_3 + La_2O_3$:Tb	3d;1055°	CaS	0	0	
	50	$CaCO_3 + La_2O_3$	8d;1050°	CaS	0	0	
	54	$CaCO_3 + La_2O_3$	8d;1060°	CaS	0	0	
	66	$CaCO_3 + La_2O_3$	8d;1055°	CaS	0	0	
	67	$CaCO_3 + La_2O_3$	8d;1050°	CaS	0	0	
$SrLa_2S_4$	16	$SrCl_2 + La_2O_3$	4d;1050°	SrS	0	0	
	30	Batch 28	2d;1120°	0	0	0	
$SrNd_2S_4$	44	$SrCO_3 + Nd_2O_3$	2d;1120°	SrS, Nd_2S_3	?	0	
	56	$SrCO_3 + Nd_2O_3$	8d;1050°	?	?	?	
	56[1]	$SrCO_3 + Nd_2O_3$	8d;1050°	?	?	?	
$CaPr_2S_4$	43	$CaCO_3 + PrCl_3 \cdot 7H_2O$	2d;1120°	Pr_2S_3, CaS	0	0	
$CaNd_2S_4$	55	$CaCO_3 + Nd_2O_3$	8d;1055°	CaS	0	0	
$CaGd_2S_4$	61	$CaCO_3 + Gd_2O_3$	8d;1060°	?	0	0	
$SrGd_2S_4$	75	$SrCO_3 + Gd_2O_3$	In progress	---	---	---	
$CaHo_2S_4$	63	$CaCO_3 + Ho_2O_3$	8d;950°	Mixed structure phases resulted w/Yb_3S_4-type			
	68	$CaCO_3 + Ho_2O_3$	In progress	---	---	---	
$YbLa_2S_4$	82	$Yb_2O_3 + La_2O_3$	In progress	---	---	---	

Table 11

Synthesis of Other Ternary Sulfides

Compound	Run and Number	Starting Material	Conditions	Phases (trace unless noted)			Comments
		$CaFe_2O_4$ Types					
$SrDy_2S_4$	74	$SrCO_3 + Dy_2O_3$	In progress	---	---	---	
$SrEr_2S_4$	60	$SrCO_3 + Er_2O_3$	8d;1060°	?	?	?	
$SrHo_2S_4$	51B	$SrCO_3 + Ho_2O_3$	8d;1060°	SrS,HoS	0	0	
	76	$SrCO_3 + Ho_2O_3$	In progress	---	---	---	
$SrTb_2S_4$	77	$SrCO_3 + Tb_4O_7$	In progress	---	---	---	
$SrTm_2S_4$	53	$SrCO_3 + Tm_2O_3$	8d;1060°	SrS,TmS	0	0	
	78	$SrCO_3 + Tm_2O_3$	In progress	---	---	---	
SrY_2S_4	79	$SrCO_3 + Y_2O_3$	In progress	---	---	---	
$SrYb_2S_4$	80	$SrCO_3 + Yb_2O_3$	In progress	---	---	---	
		Spinel Type					
$ZnAl_2S_4$	81	$ZnO + Al_2O_3$	In progress	---	---	---	
		MnY_2S_4 Type					
$CaEr_2S_4$	57	$CaCO_3 + Er_2O_3$	8d;1050°	ErS,CaS	0	0	R
	57[1]	$CaCO_3 + Er_2O_3$	8d;950°	CaS	0	0	R
$CaTm_2S_4$	62	$CaCO_3 + Tm_2O_3$	8d;950°	?	?	?	
CaY_2S_4	64	$CaCO_3 + YCl_3$	8d;950°	?	?	?	No product
$CaYb_2S_4$	65	$CaCO_3 + Yb_2O_3$	8d;950°	?	?	?	
$MgEr_2S_4$	52	$MgCO_3 + Er_2O_3$	8d;1060°	?	?	?	
	69	$MgCO_3 + Er_2O_3$	In progress	---	---	---	
$MgHo_2S_4$	58	$MgCO_3 + Ho_2O_3$	8d;1050°	0	0	0	R
	83	$MgCO_3 + Ho_2O_3$	In progress	---	---	---	Large batch
MgY_2S_4	42[1]	$MgCO_3 + YCl_3$	8d;1050°	?	0	0	No product
	71	$MgCO_3 + Y_2O_3$	In progress	---	---	---	

Table 11
(Continued)

Synthesis of Other Ternary Sulfides

Compound	Run and Number	Starting Material	Conditions	Phases (trace unless noted)			Comments
$MgTb_2S_4$	70	$MgCO_3 + Tb_4O_7$	In progress	---	---	---	
$MgYb_2S_4$	72	$MgCO_3 + Yb_2O_3$	In progress	---	---	---	
$MnHo_2S_4$	59	$MnO_2 + Ho_2O_3$	8d;1050°	HoS,MnS	0	0	No product
$MnEr_2S_4$	39[1]	$MnO_2 + Er_2O_3$	8d;1050°	MnS,ErS	0	0	No product
	73	$MnO_2 + Er_2O_3$	In progress	---	---	---	

atmosphere. We will withhold final judgment until our exploratory work is complete, but the preliminary finding is that these compounds seem to have less desirable characteristics than do other ternary sulfide families.

New synthesis experiments have been started on the spinel family of compounds. $ZnAl_2S_4$ is a prototype example. Many thiospinels have been prepared in various laboratories and the materials are much better known than are the other ternary sulfides. Synthesis is not expected to be a major difficulty.

Thermal Stability

We know that the ternary sulfides are stable to 1000-1100°C because that is the temperature of synthesis. The hot-pressing work has established that $CaLa_2S_4$ is stable at least to 1600°C and maybe 1800°C. What is not known is whether there are small losses due to partial volatilization of the materials and if vapor losses would lead to non-stoichiometry and degraded optical properties. The experience with the black hot-pressed materials suggests that this is the case.

New experiments are being set up to fire small pellets of the various ternary sulfides (a) in flowing argon, (b) in air and (c) in flowing H_2S at various temperatures and to follow any weight losses as a function of time. In this way both vaporization of the materials and the temperature at which the kinetics of oxidation becomes important will be known.

This work was only started at the end of the quarter with some furnaces being set up.

Chemical Vapor Deposition

CVD experiments using closed silica tubes with iodine as a transport medium are underway on some of the ternary sulfides, initially those with the MnY_2S_4 structure. Hot zone temperatures of 900°C and a 100° thermal gradient to the cold end have produced some acicular crystals a few mm in length and fractions of a mm in cross-section. Experiments at higher temperatures are continuing.

SPECTROSCOPIC MEASUREMENTS

IR Transmission and Lattice Vibrations

A slab of hot-pressed $CaLa_2S_4$, black as it came out of the hot press, was re-fired in H_2S with the production of a translucent, gray material. The re-fired material transmits somewhat in the infrared, in contrast to the as-pressed piece which was opaque. Figure 17shows the direct transmission spectrum through the 1 mm thick slab. There is a distinct IR cutoff at about 18 μm. The absorption feature at 11 μm may well be due to sulfate impurities introduced during the re-firing. This point will need to be investigated further. Figure 17 does confirm the initial hypothesis that $CaLa_2S_4$ and by implication the other Th_3P_4 structure ternary sulfides will transmit in the 8-20 μm region providing that the problem of blackening can be overcome. This problem will be addressed vigorously as soon as the next lot of hot-pressed pieces are available.

Infrared spectra have been measured on some examples of the other ternary sulfides by powder techniques on a conventional Perkin-Elmer Model 621 spectrometer. Some typical results are shown in Figs18,19, and 20. The spectra are only meaningful down to 300 cm^{-1} (33 μm) because of the strong absorption of KBr at longer wavelengths. Only one of the compounds, $SrTm_2S_4$ with the $CaFe_2O_4$ structure has a distinct absorption band in this wavelength region. All show

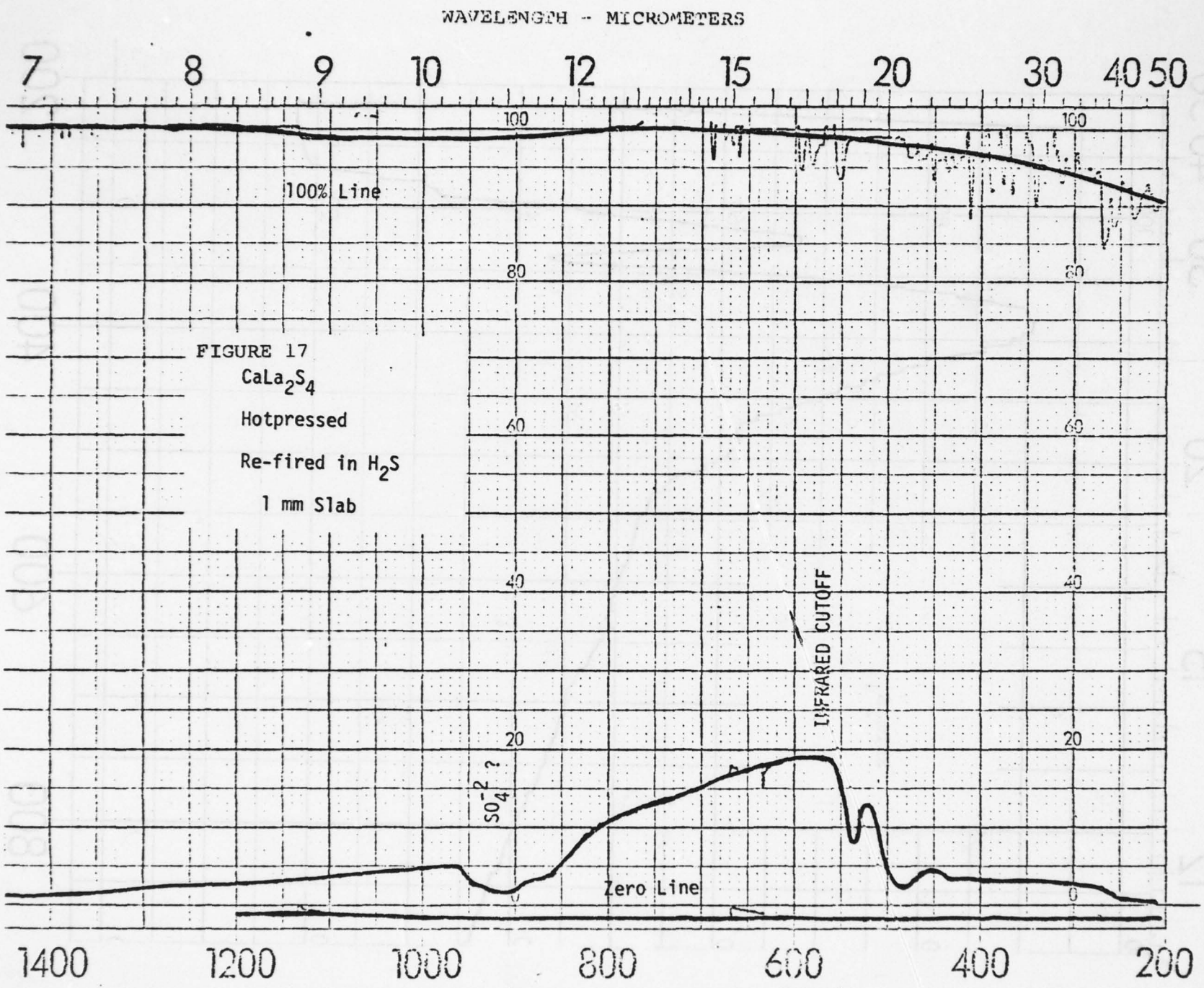


FIGURE 17

$CaLa_2S_4$

Hotpressed

Re-fired in H_2S

1 mm Slab

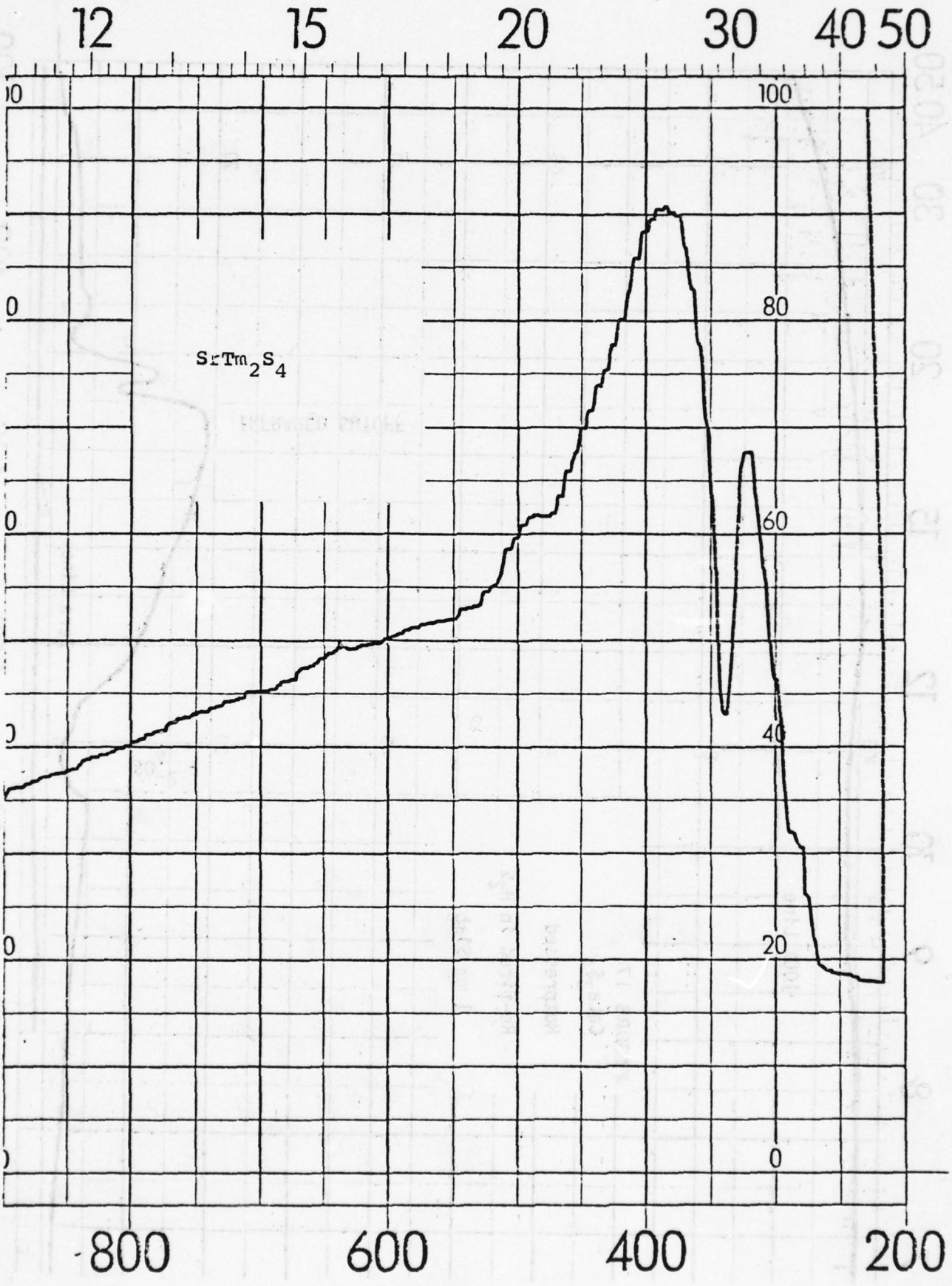


Figure 18 Powder IR spectrum of $SrTm_2S_4$ with the $CaFe_2O_4$ structure.

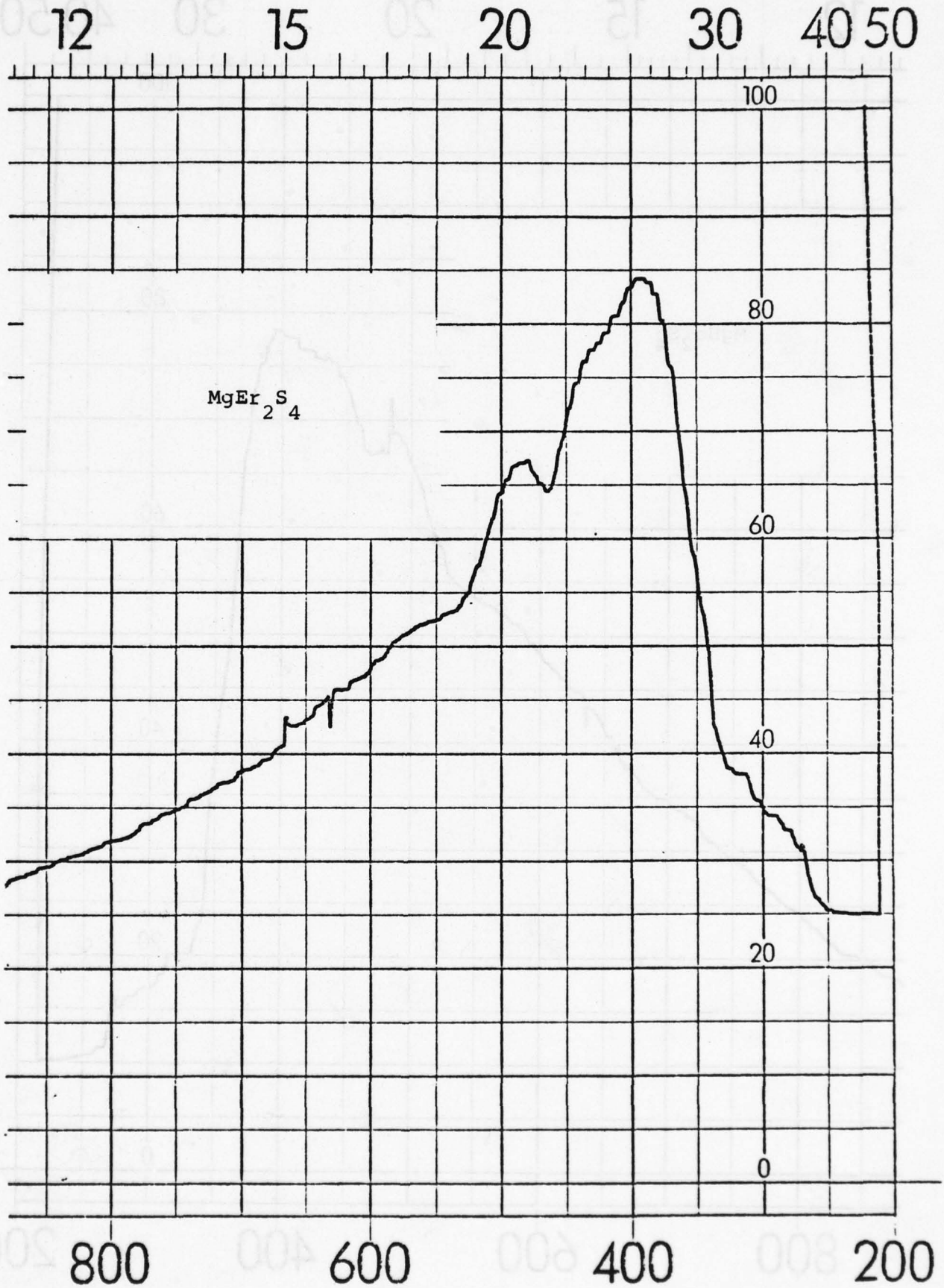


Figure 19 Powder IR spectrum of $MgEr_2S_4$ with the MnY_2S_4 structure.

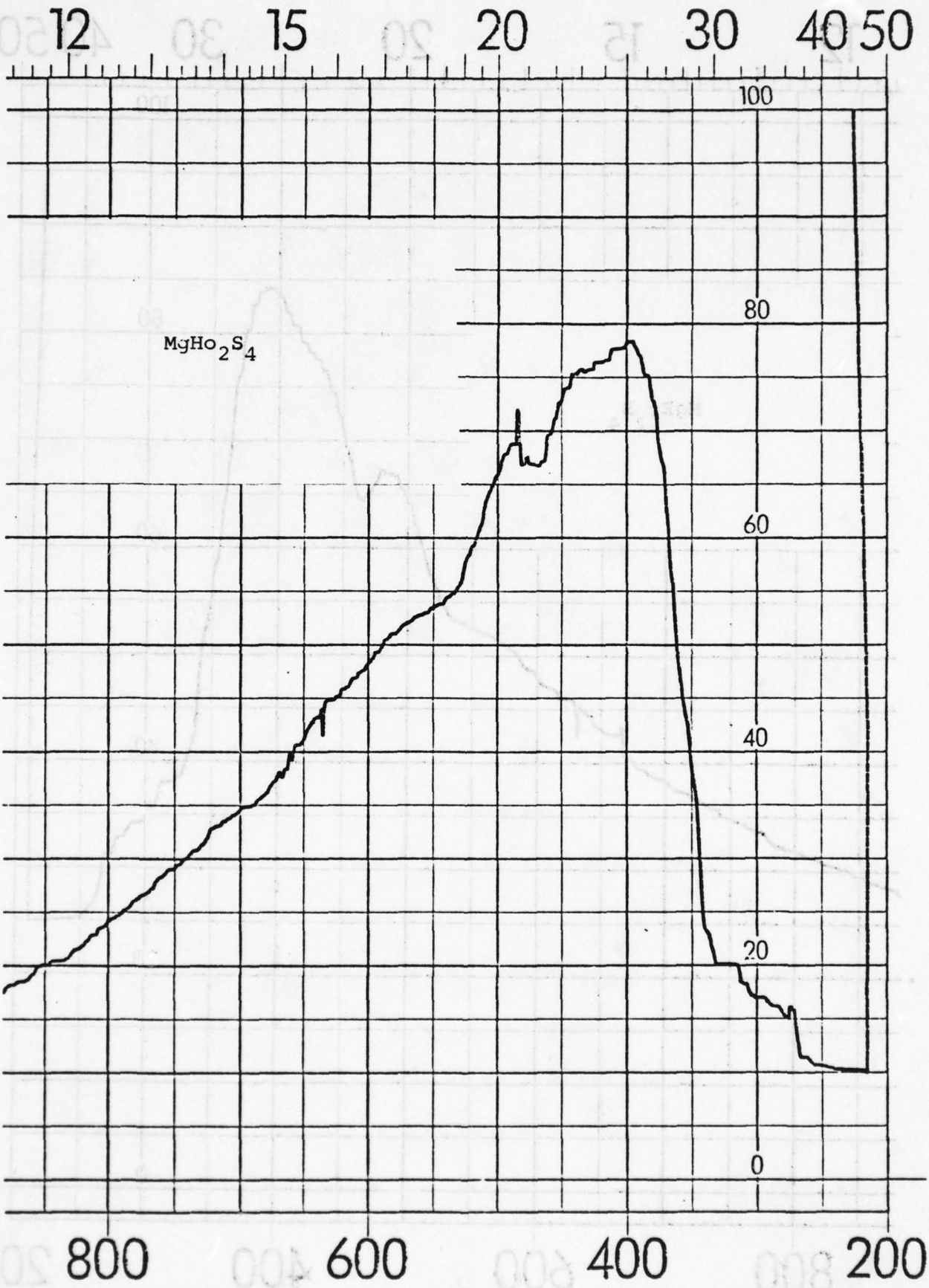


Figure 20 Powder IR spectrum of $MgHo_2S_4$ with the MnY_2S_4 structure.

a gradual cut-off between 25 and 30 μm. It is unlikely that a bulk specimen would transmit so far out into the infrared and the cut-off would be expected at higher frequencies.

In an effort to determine low frequency phonon modes in these materials, Raman spectra were measured on pressed powder specimens. One result each for a $CaFe_2O_4$ structure ($SrTm_2S_4$) and a MnY_2S_4 structure ($MgEr_2S_4$) are shown in Figs.21 and 22. The highest frequency phonon modes active in the Raman effect occur at 350 cm^{-1}. The Raman bands for the $CaFe_2O_4$ compounds are sharp and there are many of them as predicted by the rather complicated crystal structure. $MgEr_2S_4$ exhibits only three rather broad bands and these remain broad down to liquid nitrogen temperature. Some workers have claimed that the MnY_2S_4 structure is disordered with a random distribution of divalent cations and rare earth cations over the available sites. The Raman spectra support this view, the spectrum being the expected pattern for a highly disordered structure.

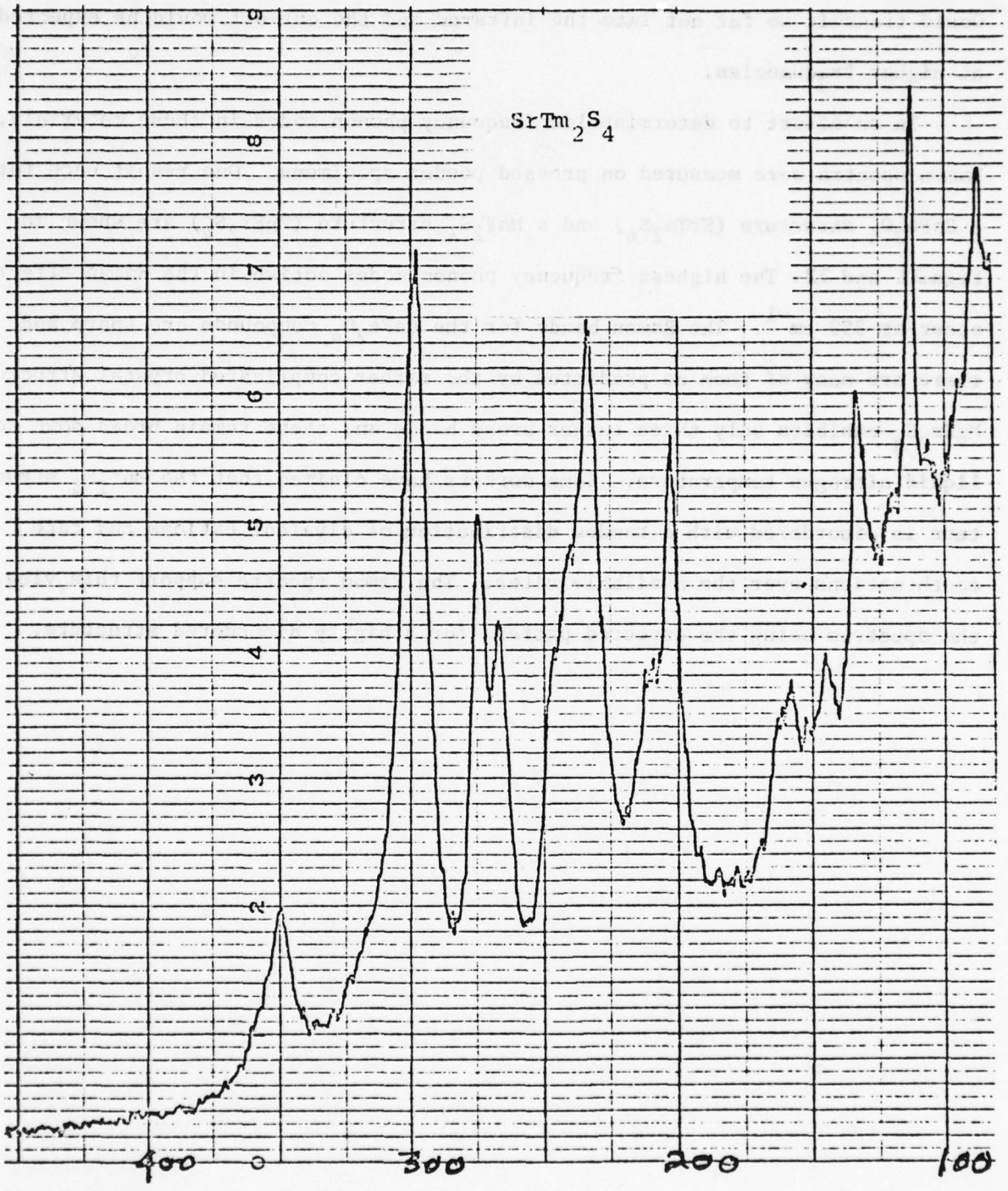


Figure 21 Raman spectrum of $SrTm_2S_4$ with the $CaFe_2O_4$ structure.

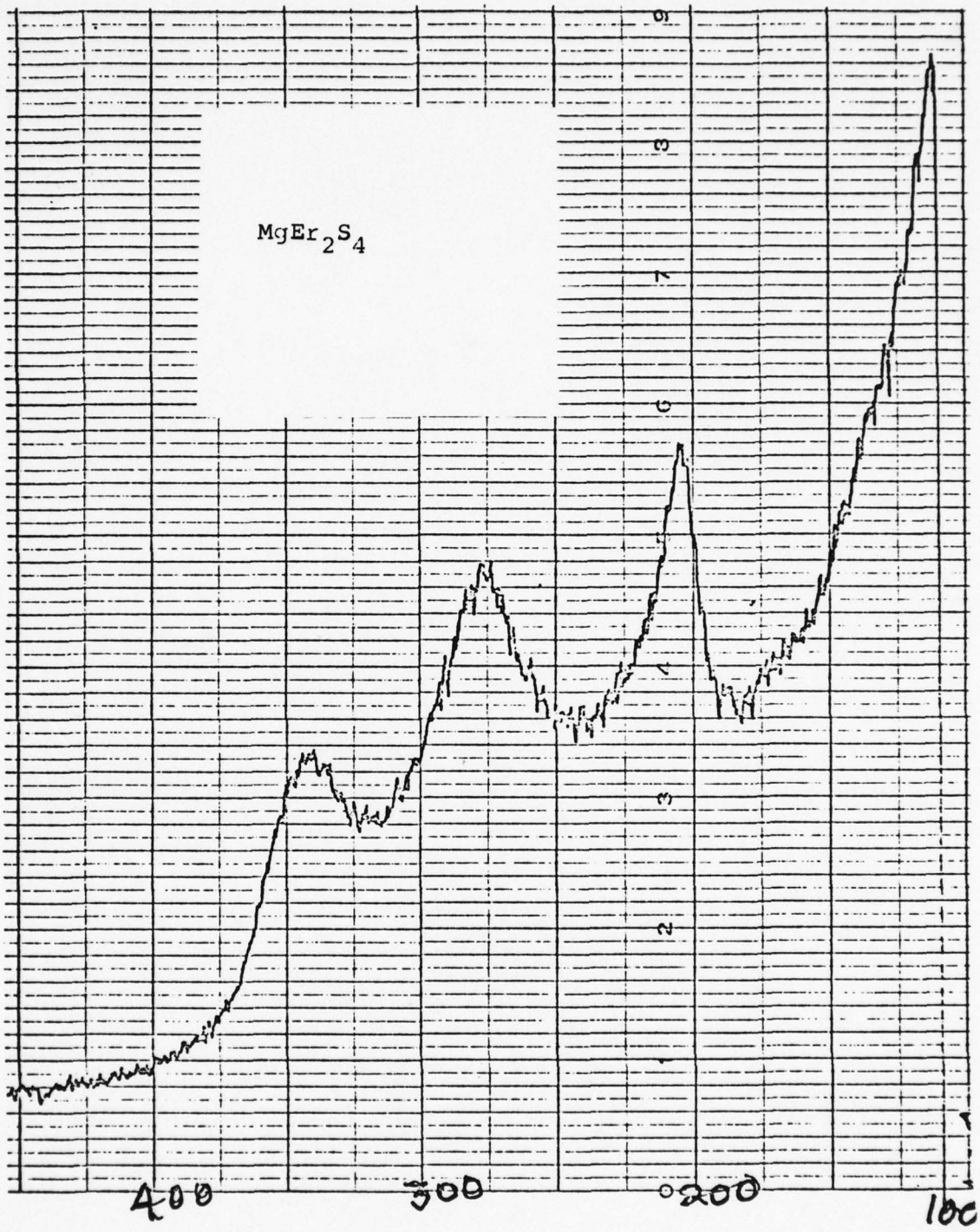


Figure 22 Raman spectrum of $MgEr_2S_4$ with the MnY_2S_4 structure.

PRECEDING PAGE BLANK-NOT FILMED

TASK 2.0 FRACTURE TOUGHNESS ENHANCEMENT

THIS SECTION WAS PREPARED BY

R. M. CANNON, JR.

TASK 2.0 Fracture Toughness Enhancement

An evaluation was made of possible toughening systems for the various candidate window materials. Table 12 summarizes the results of this analyses.

TABLE 12
TOUGHENING SYSTEMS

TASK NO.	SPECIFIC SYSTEMS	REMARKS
1.1	$ThO_2 \cdot GeO_2$ $2ZnO \cdot GeO_2$	Probably in equilibrium with ZrO_2 but $\frac{\Delta n}{n} \sim 0.12$ marginal for IR.
	$CaAl_4O_7$, $SrAl_4O_7$	Probably react with ZrO_2.
1.2	$2Nb_2O_5 \cdot Ta_2O_5$	Probably reacts with ZrO_2.
	$HfTiO_4$	Probably in equilibrium with ZrO_2 or HfO_2, index match unknown.
		For both need fine grain size to prevent microcracking and get best K_c possible.
1.3	$3Al_2O_5 \cdot 2SiO_2$	ZrO_2 in equilibrium - good chance of success - but $\Delta n/n \approx 0.25$, radar only. (Could perhaps add mica - for microcracks, tune $\Delta n/n$ (by tuning mica).)
	$3Ga_2O_3 \cdot GeO_2$	Likely $\Delta n/n$ much less ~ 0.1.
	$ZrSiO_4$ $HfSiO_4$	In equilibrium with ZrO_2/HfO_2. $\Delta n/n \sim 0.1$, marginal.
	$B_4Al_{18}O_{33}$	Probably ZrO_2 in equilibrium but $\Delta n/n$ high.
	$Cs_2O \cdot Al_2O_3 \cdot 4SiO_2$	ZrO_2 equilibrium not known, $\Delta n/n$ high. (Could perhaps add mica - for microcracks, tune $\Delta n/n$ (by tuning mica).)

TABLE 12 (cont.)
TOUGHENING SYSTEMS

TASK NO.	SPECIFIC SYSTEMS	REMARKS
1.4	ZrO_2-ZrO	Toughening demonstrated $K_c > 6$ MN/m$^{3/2}$. Δ n/n match should be fair to good, optimum K_c for d = 1000-3000 Å
	ThO_2-ZrO_2	Toughening to K > 5 MN/m$^{3/2}$ Δ n/n ~ 0.035 - requires $d/\lambda_o < 20$-30.
1.5	$BeSiN_2$-AlN	Coherent precipitates being investigated, ZrO_2 Δ n/n good for AlN. Matrix birefrigence may limit permissible grain size.
1.6	β-Sialon	Toughen with ZrO_2, possibly tune Δ n/n, equilibrium with ZrO_2 unknown. Matrix birefrigence may limit permissible grain size.
1.7	Sulfides	Layer structure precipitates for cleavage
Others	$BeSiN_2$-AlN or β-Sialon	Glassy, wetting, non absorbing grain boundary phase ⇒ pull out toughening. Possible use of wurtzitic BN, ultra fine particle size.
	Al_2O_3 + Cr_2O_3 alloy + ZrO_2 particles	Can tune Δ n/n ~ 0. Plus, alloy has lower CTE, higher H than Al_2O_3. Probably higher IR cut off than alumina.

TASK 3.0 THERMOSTRUCTURAL ANALYSES

TASK 3.0 Thermostructural Analysis

Table 13 lists six(6) reference materials which have been selected as standards of comparison for thermostructural testing. These represent current and/or advanced materials contemplated as electromagnetic windows for several DoD missile systems.

A thermostructural model has been formulated for predicting both temperature and structural responses for a point-loaded disc. Typical temperature predictions for three (3) classes of ceramic materials which span current materials under study (with regard to thermal and mechanical properties) are shown in Figure 23 for identical thermal loadings. The severity of lateral temperature gradients correlate directly with each materials thermal diffusivity and draw attention to the importance of this property in determining each materials resistance to thermal shock. Figure 24 presents the corresponding predicted finite-element stress predictions. For the specified thermal loading, the carbide-based ceramic is predicted to have the lowest tensile hoop stress.

It is planned to make pre-test thermostructural predictions for each promising candidate under representative thermal loadings typical for missile system EM windows or enclosures on advanced systems of interest to this program. Similar predictions will also be made for selected reference materials listed in Table 13 for comparison. These data will be compared with experimental data as described in the first quarterly report.

TABLE 13

Re-entry & Environmental Systems Division

REFERENCE MATERIALS
FOR
COMPARATIVE THERMAL SHOCK TESTS

MATERIAL	λ CUT-OFF (um)	CTE ($^1/C^o$)	KNOOP$_{100}$ kg/mm^2	T_{DECOMP} (^oC)	ϵ, tan (8.5GHz)	RANGE*
Spinel (Cz)	6.1	7.4×10^{-6} (25-800°C)	1275	2145 (M)	8.3, 0.00001	V, IR, M
Sapphire (Cz) 0° and 60°- Type M	6.8	7.7×10^{-6} (20-500°C)	1910-2185	2040 (M)	9.4, 0.00002	V, IR, M
Pyroceram™ (9606) Fortified, Unfortified	-	5.7×10^{-6} (20-320°C)	698	1350 (M)	5.5, 0.00033	M
Silicon Nitride (Hot Pressed NC-132)	-	3.3×10^{-6} (20-1300°C)	1800	1700° (V)	8.3, 0.004	M
Raytran™ ZnSe	14.0	7.6×10^{-6} (20-170°C)	100 (50g)	1520 (M)	-	LWIR
Raytran™ ZnS	12.0	7.9×10^{-6} (20-500°C)	250 (50g)	1830 (M)	-	LWIR

*V - visible
IR - infrared
M - microwave
LWIR - far infrared

FIGURE 23

Chemistry & Environmental Systems Division

PREDICTED TEMPERATURE GRADIENTS USING THE 3-D THT PROGRAM WITH TEMPERATURE-DEPENDENT INPUT THERMAL PROPERTIES

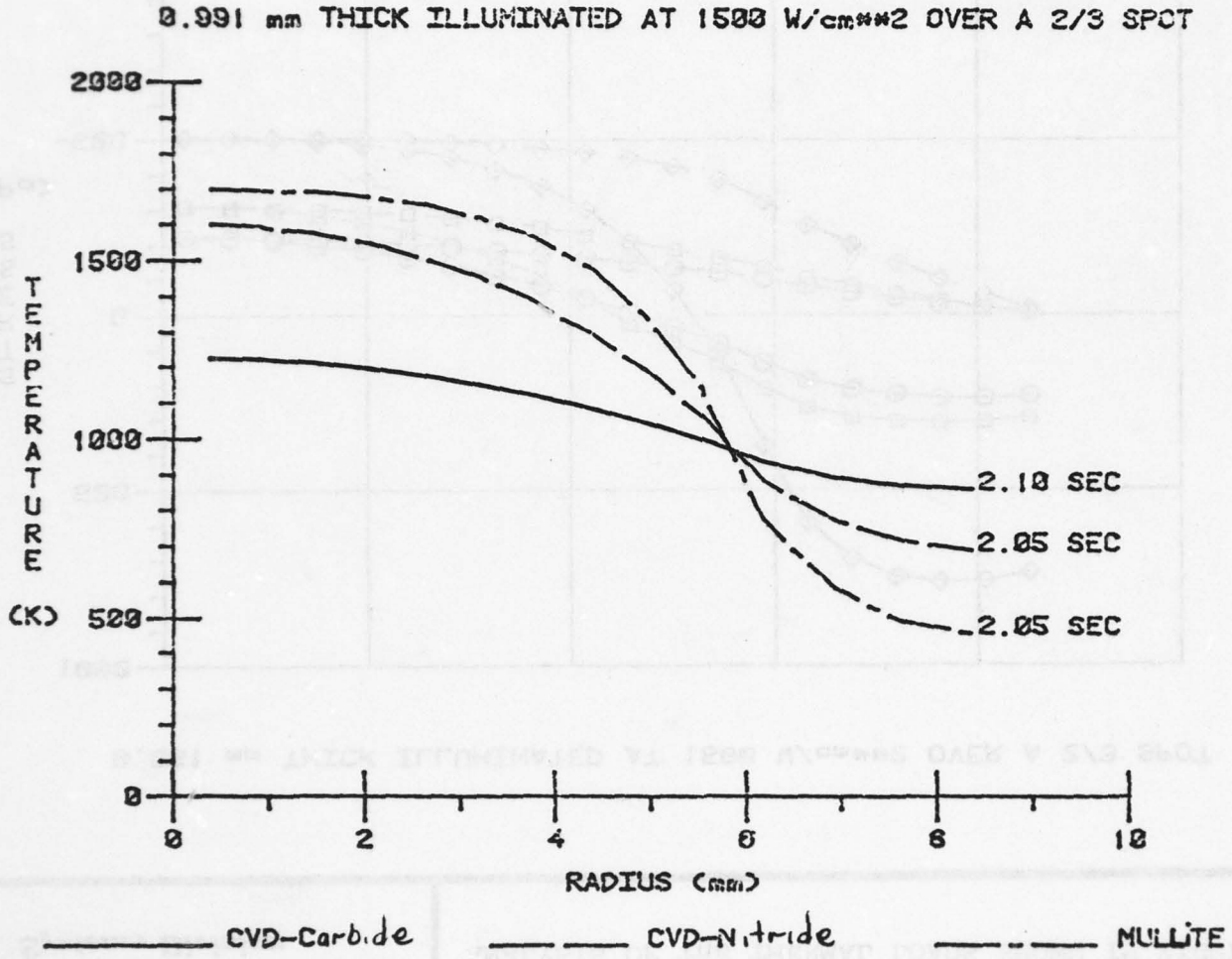
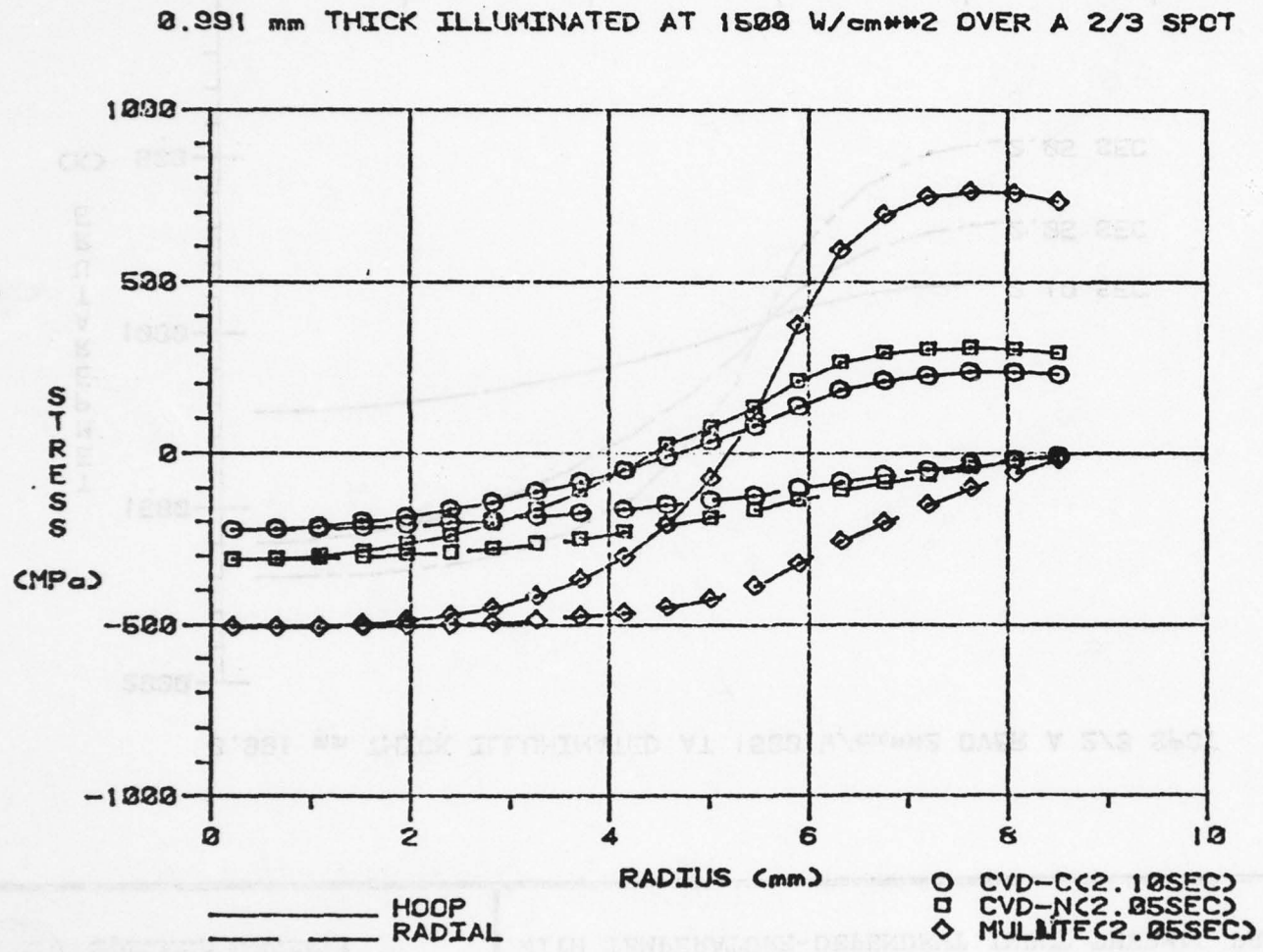


FIGURE 24

Re-entry & Environmental Systems Division

PREDICTED THERMAL STRESSES BASED ON A FINITE-ELEMENT ANALYSIS OF THE THERMAL LOADS SHOWN IN FIGURE 23.



TASK 4.0 MODELLING

OPTICAL MODELLING OF GLOBULAR INCLUSIONS

THIS SECTION WAS PREPARED BY

W. A. HARRISON

TASK 4.0 - MODELLING

OPTICAL MODELLING OF GLOBULAR INCLUSIONS

SUMMARY

We extend the earlier analysis of optical scattering to small inclusions of modified refractive index, and evaluate the results for parameters appropriate to 20% addition of ZrO_2 to ThO_2, dispersed as three micron inclusions.

It is found that microwaves have a negligible effect from these inclusions. On the other hand the system will be white - no image transmitted - to light and IR. To reduce blurring of one-micron light to five degree deflections or to reduce in line intensity loss to 10% would require inclusions either less than 900 Å (0.09 u) or greater than 0.4 cm. (nearly the thickness of the specimen). Blurring is the problem for large particles, but intensity loss is the problem for small particles.

Otherwise it is necessary to match the refractive index of the inclusion to that of the host. The angular dispersion is directly proportional to the discrepancy in refractive index, $\Delta n/n = -.03$ for $ThO_2(ZrO_2)$. Thus a discrepancy of less than 0.002 is required to reduce the blurring to less than 5^o and less than 0.0004 to reduce it under one degree for inclusions of a few microns.

We earlier modeled the optical properties of polycrystalline materials using random close-packed spheres, of diameter d, packed like marbles in a bag, with the refractive index of the interstitial regions and of half the spheres given by n and that of the other half of the spheres with refractive index given by $n + \Delta n$. We now extend that analysis to obtain the effect of small globular inclusions of a second phase material. It is an obvious extension of the model: if the inclusions have diameter d we again model the system as close-packed spheres of diameter d and if the volume fraction of the material constituting these inclusions is x we let the fraction x of the spheres have index $n + \Delta n$. This should give a very good representation of the system and probably could not be improved upon without further experimental characterization of the system.

The mathematics is only slightly changed. Again the probability of a ray of wavenumber k scattering by an angle θ given by $\cos\theta = 1 - q^2/(2k^2)$ is from the earlier Eq. 3,

$$P(\theta) \cdot \frac{4k^4}{q^6 A}\left(\frac{\Delta n}{n}\right)^2\left(\frac{qd}{2}\cos\frac{qd}{2} - \sin\frac{qd}{2}\right)^2\left|\sum_j e^{-iq\cdot r_j}\right|^2 \qquad (1)$$

where A is the cross-sectional area of the specimen and the sum is over the positions r_j of the spheres of refractive index $n = \Delta n$. The value of that sum, given in the earlier Eq. 6, becomes

$$\left|\sum_j e^{-iq\cdot r_j}\right|^2 = \sum_{ij} e^{-iq\cdot(r_i - r_j)} = Nx - \frac{3Nx^2}{(qr_0)^2}\left(\frac{\sin qr_0}{qr_0} - \cos qr_0\right) \qquad (2)$$

when only a fraction x of all spheres are included. In comparison to the sum over all spheres the first contribution is from terms in the double sum for which i = j, and is reduced by x; the second contribution is from terms for which $i \neq j$ and is reduced by x^2. (In the earlier analysis we inadvertantly multiplied both by $x^2 = \frac{1}{4}$, and this correction should be made to the earlier results. It does not qualitatively change our conclusions but would change the results in detail.) A suitable value for r_0 was obtained from $4\pi r_0^3/3 = d^3$.

The value of Eq. 2 is Nx(1-x) at small q; it rises above Nx at larger q and finally oscillates around Nx, approaching it asymptotically as q becomes very large. With limited volume fraction of inclusions, say less than 30%, it should be perfectly suitable to take this expression as constant at Nx. We shall do that though there would be little difficulty in keeping the full form if it seemed important.

The consequences of Eq. 1 are then rather simple in the two interesting limits. In the case of microwaves the wavelength will always be larger compared to d so kd and qd can be taken very small in Eq. 1. In the case of light and IR the wavelength will always be short compared to d and we may take kd large in Eq. 1. These are the two limits we discussed in detail also for the polycrystalline case.

Microwaves. For qd small $\frac{qd}{2}\cos\frac{qd}{2} - \sin\frac{qd}{2}$ approaches $-(qd)/24$. N is the number of spheres, equal to At/d^3, where t is the thickness of the specimen so Eq. 1 becomes

$$P(G) = \frac{x}{144}\frac{t}{d}\left(\frac{\Delta n}{n}\right)^2 (kd)^4 \qquad (3)$$

The scattering of the light is independent of angle θ, which means that it simply acts to reduce the intensity of the image and increase the background. The most useful number, then, is the fractional reduction in intensity, $\Delta I/I$ obtained from Eq. 3 by integrating over solid angle;

$$\frac{\Delta I}{I} = \frac{\pi}{36}\frac{xt}{d}\left(\frac{\Delta n}{n}\right)^2 (kd)^4 \qquad (4)$$

Using values representative of ZrO_2 in ThO_2 we may take $x = \neq 0.20$, $\Delta n/n = 0.03$, particle size of d = 3 microns, and t = 0.5 cm to obtain $\Delta I/I = 0.026\ (kd)^4$. For a wavelength of 1 cm, this is 3×10^{-13} and is completely negligible. For microwaves we need not worry about the scattering from inclusions.

Light and IR. We shall refine our evaluation of this limit since it is of considerable importance. Here kd is large and correspondingly we took qd large in Eq. 1 to approximate $(\frac{qd}{2}\cos qd - \sin\frac{qd}{2})^2$ by $(qd)^2/8$, which leads to

$$P(\theta) = \frac{1}{2}\frac{t}{d}\left(\frac{\Delta n}{n}\right)^2 \frac{\chi}{\theta^4} \qquad (5)$$

The scattering is predominantly at very small angles, corresponding to a blurring of the image rather than a reduction in intensity. We made a crude estimate of the mean square angular scatter, as a measure of this blurring, for this limit, and then made a numerical evaluation in the earlier analysis.

We return to Eq. 1, again using only the first term of Eq. 2 for the final factor. We proceed now to an evaluation of the mean square angular deflection $\theta = \theta\ P(\theta)\ 2\ \sin\theta\ d\theta$. This can be written as in integral over q by noting that $\sin\theta\ d\theta = qdq/k^2$ and we may replace θ by q^2/k^2, valid at small angles and reasonably close over the entire angular range. Note also $N = tA/d^3$. We easily obtain

$$\langle\theta^2\rangle = 8\pi\chi t\left(\frac{\Delta n}{n}\right)^2 \int_0^{2kd} dq\left(\frac{qd}{2}\cos\frac{qd}{2} - \sin\frac{qd}{2}\right)^2 \Big/ qd^3$$

$$= 2\pi\chi\frac{t}{d}\left(\frac{\Delta n}{n}\right)^2 f(kd) \qquad (6)$$

where f(kd) is given by

$$f(kd) = \int^{kd} du\,(u\cos u - \sin u)^2/u^3$$

where f(kd) is given in Table14 as a function of d/λ:

d = inclusion diameter
t = window thickness
λ = light wavelength
x = volume fraction of additive
$\Delta n/n$ is discrepancy in refractial index

In the last step we changed the dummy variable in the integration to u = qd/2.

In our earlier analysis we gave $f(kd) = \frac{1}{4}\ln\frac{kd}{2}$, but we now improve upon that. The integral in Eq. 7 can be carried out to obtain

$$f(kd) = \frac{\cos(2kd)-1}{(2kd)^2} + \frac{\sin 2kd}{2kd} - \frac{1}{2} + \frac{(2kd)^2}{4\cdot 2!} - \frac{(2kd)^4}{8\cdot 4!} + \frac{(2kd)^6}{12\cdot 6!} - \cdots \quad (8)$$

and we will tabulate the results of the evaluation. It will be most convenient, however, to give the results in terms of the ratio of inclusion diameter to wavelength, $d/\lambda = kd/(2\pi)$. In these terms we give in Table14 f(kd) for d/λ from zero to 0.3. Quite accurate forms for larger d/λ and for d/λ quite small are given by

$$f(kd) \approx \frac{1}{2}\ln(5.16\, d/\lambda) \quad \text{for } d/\lambda > 0.3 \quad (9)$$

$$f(kd) \approx 43.3\,(d/\lambda)^4 \quad \text{for } d/\lambda < 0.2 \quad (10)$$

The message is rather clear. Unless the diameter of the inclusions is considerably less than the wavelength, which seems unlikely either in the optical region or in the IR, f(kd) is of order unity. For the parameters given earlier for ZrO_2 in ThO_2, the leading factor in Eq. 6 is 1.88 radians , corresponding to a root mean square angular deviation of 80°, essentially completely diffuse transmission.

TABLE 14

CALCULATION FOR f(kd)

d/λ	f(kd)	d/λ	f(kd)
0	0	0.4	0.36
0.02	6.91×10^{-6}	0.6	0.57
0.04	1.10×10^{-4}	0.8	0.71
0.06	5.51×10^{-4}	1.0	0.82
0.08	1.71×10^{-3}		
0.10	4.11×10^{-3}		
0.12	8.32×10^{-3}	2	1.17
0.14	1.50×10^{-2}	4	1.51
0.16	2.48×10^{-2}	6	1.72
0.18	3.83×10^{-2}	8	1.86
0.20	5.61×10^{-2}	10	1.97
0.22	7.85×10^{-2}		
0.24	0.106		
0.26	0.139	100	3.12
0.28	0.176	1000	4.27
0.30	0.218	10^n	1.15n + 0.82

We might next ask what circumstances would lead to a more suitable window. For 20% inclusions with $\Delta n/n$ of 0.03 and a window thickness of 0.5 cm we may readily show that one can only obtain a blurring of less than 5° if the inclusion diameter is greater than 0.4 cm. Alternatively, for a 10% intensity loss for small particles, equation (4), diameter of the second phase particles must be <900 Å. Furthermore, we see from equation 6 that the angular blurring (the square root of equation 6) depends only on the square root of the concentration and linearly on the $\Delta n/n$.

TASK 5.0 CONTINUING SEARCH FOR IMPROVED MATERIALS

THIS SECTION WAS PREPARED BY:

G. A. SLACK

I. Review of Progress to Date

A survey of the literature on optically transparent materials for use as high temperature windows has been carried out. As a result a small number of potential candidates were chosen for exploration at the R&D Center. These are $Al_6Si_3O_{13}$ (mullite), $Al_{18}B_4O_{33}$ (aluminum borate), $AlNbO_4$ (aluminum niobate), $BeSiN_2$ (beryllium silicon nitride), Y_2O_3 (yttria), and ThO_2 (thoria). The first three were chosen because of previous success with making transparent Al_2O_3. They represent possible extensions of the present state of the ceramic art. The $BeSiN_2$ was chosen as the best metal nitride that can be synthesized in a useful crystal structure without the necessity of employing a diamond press. The Y_2O_3 and ThO_2 were chosen because they are cubic in structure, have a large range of infrared transparency, and posses high melting temperatures.

Powders of all of these have been successfully synthesized, and samples of at least 98% of theoretical density have been made by hot pressing. Pressures of less than 10^4 pounds/in^2 and temperatures less than 2000°C were sufficient for all of the oxides. The $BeSiN_2$ required pressures of 0.7×10^6 pounds/in^2 and temperatures of 1600°C to obtain the desired density.

Where necessary measurements of the thermal expansion coefficient and expansion anisotropy were made. Of the six candidates only $AlNbO_4$ exhibited sufficient anisotropy to cause microcracking in ceramic bodies. The critical grain size above which microcracking occurs is 1.5 microns. This makes good ceramic bodies difficult to obtain. Thus this material is being dropped as a potential candidate. Some pertinent data on the other candidates can be found in Table 15. Two approximate "figures of merit" appear in Table 15. The first is the ratio of thermal condcutivity to thermal expansion coefficient, and the second is the product of the hardness and the melting point. We would like both of these figures of merit to be large.

TABLE 15: Properties of Some Candidate Materials

Property	$BeSiN_2$	$Al_{18}B_4O_{33}$	$Al_6Si_2O_{13}$	Y_2O_3	ThO_2	AlN
Structure	Or, H	Or	Or	C	C	H
M, g	16.28	19.22	20.29	45.16	88.01	20.49
M.P., °K	>2300	~2200	2205	2653	3663	3070
H, kg/mm^2	2050	1340	1750	875	600	1200
$\bar{\beta}$(300°), 10^{-6}/°K	3	4.4	3.3	6.4	7.8	2.7
$\bar{\beta}$(1000°) "	7.3	6.6	5.5	8.9	8.7	6.2
$\bar{K}$(300°), W/cm°K	~1.3	~0.035	0.067	0.27	0.15	2.9
$\bar{K}$(1000°), "	~0.29	~0.022	0.042	0.06	0.038	0.64
$100\bar{K}(300°)\bar{\beta}(300°)$	43	0.80	2.0	4.2	1.9	107
$100\bar{K}(1000°)\bar{\beta}(1000°)$	4.0	0.33	0.76	0.67	0.44	10
$H\cdot(M.P.)/10^6$	>4.7	~2.9	3.9	2.3	2.2	3.7
B, 10^{11} $dyne/cm^2$	?	?	16	13.7	19.3	22
		N=55	N=21			

Or = orthorhomobic
H = hexagonal
C = cubic

The thermal conductivity of $BeSiN_2$ has been estimated by comparing its structural parameters to AlN, GaN, GaP, ZnO and $LiGaO_2$. The value given is for material where the Be and Si stoms are ordered in the lattice, the value is $\bar{K}$(300°K) ≈1.3 w/cm.deg. If the Be and Si are random on the metal sites, then the value of $\bar{K}$ could be decreased by mass fluctuation scattering to about 0.9 w/cm. deg. This will have to be measured. The thermal conductivity values of $Al_{18}B_4O_{33}$ have been estimated from those of mullite by reducing the mullite K values by $[N(\text{borate})/N(\text{mullite}]^{2/3}$, where N is the number of atoms in a primitive crystallographic unit cell. Note N-55 for $Al_{18}B_4O_{33}$ and N-21 for $Al_6Si_2O_{13}$. The thermal expansion values for $Al_{18}B_4O_{33}$ are from recent dilatometer data at the R&D Center; the microhardness values for $BeSiN_2$ and $Al_{18}B_4O_{33}$ are also recent data. From Table 15 we see that the thermal expansion properties of $BeSiN_2$, $Al_{18}B_4O_{33}$, $Al_6Si_2O_{13}$ and AlN are all similar. The values for Y_2O_3 and ThO_2 are about twice as large. So on the basis of low thermal expansion alone the first four are all comparable in quality. If we look at $\bar{K}\cdot\bar{\beta}$, then $BeSiN_2$ and AlN are better by far. The question is whether high $\bar{K}$ is needed to obtain good thermal shock resistance under the conditions encountered. In terms of H·(M.P.) all of the candidates are comparable, but $BeSiN_2$ is at the top of the list.

II. Better Candidates

Better candidate materials can be found in terms of possessing optical transparency in regions where those in Table 15 are opaque, in having higher hardness or toughness, in having lower thermal expansion coefficients, or lower anisotropy of various properties. If we can use $\bar{\beta}$, $\bar{K}/\bar{\beta}$, and H·(M.P.) as "figures of merit" let us consider fused SiO_2 glass. For this material $\bar{\beta}$=0.4, $100(\bar{K}/\bar{\beta})$=0.33 at 300°K, and $H\cdot(M.P.)10^6$=0.94. Thus in $\bar{\beta}$ it is a factor of 10 better than the other candidates, in $\bar{K}/\bar{\beta}$ it is 10 to 100 times worse, and in H·(M.P.) it is 3 times worse. Fused SiO_2 thus represents an extreme in terms of what might be done to lower $\bar{\beta}$ at the expense of the other factors. Are there other materials where $\bar{\beta}$ values of 2 to 3 x 10^{-6}/°K can be found that have high $\bar{K}/\bar{\beta}$ and H·(M.P.)? This is dealt with in the next section.

III. Low Thermal Expansion Oxides

A survey of the thermal expansion coefficients of oxide crystals and glasses has been made in an attempt to find correlations between structural parameters and low expansion. The various metallic elements occur in η-fold coordination with oxygen atoms in crystals. These η values are 3, 4, 5, 6, 8, and 12. Boron is the only element of present concern with η=3. The interatomic distances for oxides with η=4 (tetrahedral) and η=6 (octahedral) are given in Table 16. When the coordination number, η, of a metal increases the interatomic distance increases. For the change η=4 to η=6 the distance increases by 9% to 18%, an average value is about 10%. For the change η=6 to η=8 the change is also about 10%. These small changes in the equilibrium position produce large changes in the anharmonicity of the interatomic potential and hence in the thermal expansion coefficient. In Table 18 are the collected data for the thermal expansion coefficients of these metal-oxygen coordination units. Since the macroscopic thermal expansion of a crystal is a combination of the rotation plus the intrinsic expansion of these units, it will often be larger than that of the isolated units. In collecting the β values in Table 18 an attempt has been made to use only those data where the rotation effect is absent. A temperature of 1000°K was chosen so that the β values will be approximately independent of temperature.

Several observations can be made from the data in Table 18. First the unit with the lowest expansion coefficient of all appears to be the SiO_4 group with β=0.4 x 10^{-4}/°K. The other η=4 groups with $\beta \sim 1 \times 10^{-6}$/°K are BO_4, AlO_4, PO_4, VO_4, GaO_4 and possibly GeO_4. The groups MgO_4, BeO_4, ZnO_4, and LiO_4 where the metal has only a +2 or +1 charge have significantly larger β values, and (except for Be) their metal-oxygen distances are also larger. An approximate relationship holds between β, η, and Z holds for Table 18.

$$\beta = \left[\frac{(\eta-3.5)}{Z}\right] 10^{-5}/°K \qquad (1)$$

where Z = charge on the metal ion. Equation (1) says that one needs low coordination numbers and large Z to obtain low thermal expansion

TABLE 16: Octahedral and Tetrahedral Metal-Oxygen Distances in Oxide Crystals, n=4,6.

Ion	Charge State	Octahedral Distance A°	Tetrahedral Distance A°	Crystal for Octa.D.	Crystal for Tetra.D.	Ratio O.D./T.D.
Li	1	2.14	1.95	$LiVO_2$	$LiGaO_2$	1.097
Be	2	-	1.64	-	BeO	
B	3	-	1.46	-	$Zn_4B_6O_{13}$	
Na	1	2.60	2.25	$Na_2Mo_2O_7$	β-$NaFeO_2$	
Mg	2	2.11	1.92	MgO	$MgAl_2O_4$	1.099
Al	3	1.92	1.75	Al_2O_3	$AlPO_4$	1.097
Si	4	1.78	1.63	Stishovite	Cristobalite	1.092
P	5	-	1.54	-	BPO_4	
K	1	2.92	-	KVO_3	-	
Ca	2	2.41	2.03	CaO	Na_2CaSiO_4	1.187
Sc	3	2.10	-	Sc_2O_3	-	
Ti	4	1.96	1.72	TiO_2	Ba_2TiO_4	1.140
V	5	-	1.64	-	YVO_4	
Cr	6	-	1.65	-	$PbCrO_4$	
Mn	7	-	1.55	-	$KMnO_4$	
Zn	2	2.14	1.95	Rocksalt-ZnO	ZnO	1.097
Ga	3	2.00	1.78	β-Ga_2O_3	$GaPO_4$	1.124
Ge	4	1.88	1.74	GeO_2-Rutile	GeO_2-Quartz	1.080
As	5	-	1.62	-	$AlAsO_4$	
Rb	1	2.84	-	Rb_2O_2	-	
Sr	2	2.58	-	SrO	-	
Y	3	2.27	-	Y_2O_3	-	
Zr	4	2.01	-	$CaZrO_3$	-	
Nb	5	2.00	1.89	$KNbO_3$	$YNbO_4$	1.058
Mo	6	1.93	1.83	MoO_3	Ag_2MoO_4	1.055
Cd	2	2.35	-	CdO	-	
In	3	2.17	-	In_2O_3	-	
Sn	4	2.05	-	SnO_2	-	

TABLE 16: continued

Ion	Charge State	Octahedral Distance A°	Tetrahedral Distance A°	Crystal for Octa.D.	Crystal for Totra.D.	Ratio $\frac{\text{O.D.}}{\text{T.D.}}$
Cs	1	3.02	-	Cs_2O_2	-	
Ba	2	2.76	2.66	BaO	$BaZnO_2$	1.038
La	3	2.43	-	La_2O_3	-	
Lu	3	2.22	-	Lu_2O_3	-	
Hf	4	2.03	-	$SrHfO_3$	-	
Ta	5	1.99		$KTaO_3$		
W	6	1.93	1.79	Na_xWO_3	Li_2WO_4	1.078

TABLE 17: Metal-oxygen Distances for η=5,8.

Ion	Charge State	Coordination Number	Distance A°	Crystal
V	5	5	1.78	V_2O_5
Zr	4	8	2.20	Cubic ZrO_2
Hf	4	8	2.21	Cubic HfO_2
Ce	4	8	2.34	CeO_2
Th	4	8	2.42	ThO_2

TABLE 18: Thermal Expansion Data at 1000°K for Metal-Oxide Coordination Groups

Metal	Charge State	Coord. Number	β 10^{-6}/°K	Crystal	Reference
Li	1	4	19	Li_4GeO_4	1,2
Be	2	4	10.7	BeO	3
B	3	4	~1	$TaBO_4$, glass	4,5
Na	1	6	38.0	glass	5
Mg	2	6	14.3	MgO	6,7,8
Al	3	6	9.0	Al_2O_3	7,9
Si	4	6	7.2	Stishovite-SiO_2	10
Mg	2	4	2	glass	5
Al	3	4	~1	high-$AlPO_4$	11,12
Si	4	4	~1,0.4	High cristoblite-SiO_2 glass-SiO_2	5,12
P	5	4	~1	high $AlPO_4$	11,12
K	1	6	30.0	glass	5
Ca	2	6	13.6	CaO	8,13
Sc	3	6	9.7	Sc_2O_3	8
Ti	4	6	9.3	rutile-TiO_2	14
Ga	3	6	12.3	α-Ga_2O_3	15
Ge	4	6	7.8	Glass GeO_2, rutile-GeO_2	16,17
V	5	4	~1	$NdVO_4$	2,18
Zn	2	4	7.1	ZnO	19
Ga	3	4	~1	$LiGaO_2$	20
Ge	4	4	$\leq$3.3	Zn_2GeO_4	21
Sr	2	6	14.0	SrO	22
Y	3	6	8.9	Y_2O_3	8,23
Zr	4	8	12.4	cubic ZrO_2	24
Nb	5	6	3.4	α-Nb_2O_5	25
Cd	2	6	15.5	CdO	26
In	3	6	8.9	In_2O_3	27
Sn	4	6	4.4	SnO_2	8
Ba	2	6	13	BaO	28
La	3	6	9	La_2O_3	29
Ce	4	8	11.7	CeO_2	30
Lu	3	6	8.8	Lu_2O_3	8,30
Hf	4	8	11	cubic HfO_2	23
Ta	5	6	3.7	Ta_2O_5	8
W	6	6	5.1	Na_xWO_3	31,32
Th	4	8	9.8	ThO_2	33

coefficients. In addition, no unit rotations are allowed in the crystal structure. It is these units rotations that give α-quartz (SiO_2 and $AlPO_4$) α-cristobalite (SiO_2 and $AlPO_4$), pollucite ($CsAlSi_2O_4$), and many other crystals very high β values at low temperatues. We note that in the absence of rotations the macroscopis expansion is the sum of that of the individual metal-oxygen units. An exception for framework structures is explained later.

One of the mechanisms for obtaining low macroscopic β values is to use SiO_4 groups and prevent their rotation as the temperature changes. This is done in SiO_2 glass. No other techniques have so far been found to stabilize high-quartz or high-cristobalite structures at room temperature by the addition of small amounts of impurity to SiO_2. Some success in stablilizing $AlPO_4$ (high-cristobalite form) has been achieved by addition of BPO_4 and TiO_2 (Ormiston and Tanzilli, 1973). Conceivably one might use $CsAlO_2$ additions to SiO_2 in order to stabilize the high or β-cristobalite structure. $CsAlO_2$ has the cubic β-cristobalite structure, but all of the lattice vacancies are filled with Cs atoms. Here one is trying to use η=12 ions to stabilize Al and Si both in η-4 sites. This has not yet been tried. Similar kinds of impurities in $AlPO_4$ might work the same way to produce a low thermal expansion, stabilized, cubic β-cristobalite form. Such materials would have $\beta \sim 1 \times 10^{-6}/°K$, a hardness similar to that of fused SiO_2, but a thermal conductivity maybe 10 to 30 times higher. The major problem is that in all of the forms of SiO_2 or $AlPO_4$ the network of tetrahedra is formed by joining the tetrahedra only at the corners and only two tetrahedra meet at such a corner. The resulting structure is unstable against rotation or collapse. This is a fundamental problem of having two oxygen atoms for each silicon.

If one attempts to make ternary oxides of the form $SiO_2 \cdot MO_x$ where M has Z=+5 or +6 in order to take advantage of the low expansion of these high-Z units, one fails. There are no ternary compounds of tetrahedral SiO_4 groups with such oxides. There are too many oxygen atoms present, the compounds are unstable. In one such compound, SiP_2O_7, the Si has octahedral coordination with

oxygen; the SiO_4 is lost. The best one can do is use Z=4 ions with $\eta>4$ to make compounds. Examples are $ThSiO_4$, $HfSiO_4$, and $ZrSiO_4$. Here $\eta=8$ for Th, Hf and Zr. The next best method is to use Z=3 ions such as Al to make Al_2SiO_5 (sillimanite) or $Al_6Si_2O_{13}$ (mullite). The number of oxygen atoms is still too great to allow stable structures with all the metal atoms in 4 coordination. In both of these crystals 1/3 of the metal atoms (Al) are in $\eta=6$ coordination. These $\eta=6$ atoms produce most of the thermal expansion of these compounds. From Table 18 we can estimate the β of mullite at 1000°K as follows by assuming the crystal has an expansion which is the average of its constituents.

$$\beta = \frac{1}{3}\beta(AlO_6) + \frac{5}{12}\beta(AlO_4) + \frac{1}{4}\beta(SiO_4)$$

$$\beta(\text{mullite}) \simeq \left[\frac{9.0}{3} + \frac{5}{12}(1.0 + \frac{1}{4}(1.0)\right] \times 10^{-6}/°K$$

$$\beta(\text{mullite}) \simeq 3.7 \times 10^{-6}/°K$$

This is to be compared with the measured value of $5.5 \times 10^{-6}/°K$. Perhaps mullite has some internal unit rotations which are producing a value above 3.7. Mullite is considered to be a moderately good candidate material. One can also replace the Si by Ge to make germanium mullite, $Al_6Ge_2O_{13}$. This also has a moderate thermal expansion of $\beta \simeq 5 \times 10^{-6}/°K$. Other Z=3 compounds using oxides of B, Ga, In, Sc, Y, La, Lu do not appear to be as promising as the mullites.

If we proceed to the Z=2 compounds, we find the Be_2SiO_4, Zn_2GeO_4 and Zn_2SiO_4 with the phenacite structure. In these all of the ions have $\eta=4$. The Be_2SiO_4 has a high expansion with $\beta \simeq 7 \times 10^{-6}/°K$ whereas the Zn compounds have an anomalously low $\beta \simeq 3 \times 10^{-6}/°K$. The Zn compounds are promising candidates, the Be_2SiO_4 is not.

Just as $CsAlO_2$ is a "stuffed" β-cristobalite structure, one can make stuffed Al-Si-O structures. One useful example of this is $CsAlSi_2O_6$ (pollucite). Here all of the Al and Si atoms have $\eta=4$ while the Cs has $\eta=12$. We have used the large Cs ion to "force" the Al ions into the low expansion $\eta=4$ coordination. The CsO_{12} unit should have a very large thermal expansion coefficient of about $40 \times 10^{-6}/°K$. However, it is encased in a Si-Al-O framework, and

the expansion is determined by the framework. The function of the Cs is to prevent the framework from collapsing (in much the same way that it does in $CsAlO_2$). At 1000°K the β of pollucite is $\beta \simeq 3 \times 10^{-6}$/°K. This is a useful candidate.

IV. Nitrides as Stabilizers

Another approach to stabilization of SiO_2 is to replace some of the oxygen by nitrogen. In Si_3N_4 the metal-to-anion ratio is 0.75 instead of 0.50. Now the SiN_4 tetrahedra can be joined up with more than two tetrahedra meeting at each anion. This crystal structure is now very stable and no lattice collapse is found in Si_3N_4 at any temperature. In Table 19 the expansion coefficients and coordination numbers are collected for a number of nitrides. From a comparison of the $\eta=4$ groups of B, Al, and Si between nitrides and oxides it can be seen that the β values for the nitrides are 6 to 10 times higher than for the oxides. Clearly this is not desirable, thus nitrides make poorer window candidates than oxides in general.

It is possible to make mixed crystals between oxides and nitrides. The idea is to produce a crystal which is mostly oxide with just enough nitrogen to prevent the lattice instabilities. One such crystal is Si_2N_2O. Its thermal expansion (Ref. 34) is lower than that of Si_3N_4 because of the oxygen content. However, even more oxygen would be useful. This can be done in β'-sialons, which are mixed crystals of the form

$$Si_3N_4 + Al_3O_3N,$$

which make

$$Si_{6-x}Al_xO_xN_{8-x}$$

with $0 \leq x \leq 4.2$. Near the upper limit at X=4 is where half of the nitrogen is replaced by oxygen. In this whole series $\eta=4$ for both Al and Si. At X=4 the composition is $SiAl_2O_2N_2$, which is equivalent to $SiO_2 + 2AlN$. However in $SiAl_2O_2N_2$ the Si and Al are presumably random on the cation sites and the O&N are randon on the anion sites.

TABLE 19: Metal-Nitrogen Distances and Thermal Expansion Coefficients at 1000°K

Metal	Charge State	Distance A°	Crystal for Dist.	Coord. Number	α 10^{-6}/°K	Crystal for α	Ref. α
Li	1	2.15	Li_3AlN_2	4			
Be	2	1.77	hex Be_3N_2	4			
B	3	1.56	cubic BN	4	6.0	cubic BN	3
Na	1	2.45	$NaNH_2$	4			
Mg	2	2.15	Mg_3N_2	4			
Al	3	1.87	AlN	4	6.2	AlN	3
Si	4	1.74	Si_3N_4	4	4.4	Si_3N_4	34
P	5	1.58	$P_3N_3F_6$	4			
K							
Ca	2	2.44	Ca_3N_2	4			
Sc	3	2.22	ScN	6	8.1	ScN	37
Ti	3	2.12	TiN	6	10.0	TiN	8
Zn	2	~2.11	Zn_3N_2	4			
Ga	3	1.94	GaN	4	5.0	GaN	35,36
Ge	4	1.84	Ge_3N_4	4			
Sr	2	2.72	SrNH	6			
Y	3	2.44	YN	6			
Zr	4	2.30	ZrN	6	8.2	ZrN	8
In	3	2.15	InN	4	~4	InN	36
La	3	2.65	LaN	6			
Lu	3	2.38	LuN	6			

TABLE 20. Metal-Carbon Distances and Thermal Expansion Coefficients at 1000°K

Metal	Charge State	Distance A°	Crystal	Coord. Number	α 10^{-6}/°K	Crystal for α	Ref. for α
Be	2	1.87	Be_2C	4			
B	3						
Mg	2	2.31	$Mg(CH_3)_2$	4			
Al	3	2.12	Al_4C_3	4			
Si	4	1.88	SiC	4	5.3	SiC	3
Ti	?	2.16	TiC	6	8.1	TiC	8
Zr	?	2.32	ZrC	6	7.6	ZrC	8
Hf	?	2.23	HfC	6	7.0	HfC	8
Ta	?	2.23	TaC	6	6.8	TaC	8
W	?	2.20	WC	6	5.1	WC	8

The β of $SiAl_2O_2N_2$ is nearly isotropic and has been measured as $\beta=2.45 \times 10^{-6}/°K$ at around room temperature (Ref. 38). The estimated value at 1000°K using averages over oxygen and nitrogen tetrahedra from Tables 18 and 19 is $\beta(\text{estimate}) = 3.2 \times 10^{-6}/°K$. The agreement here with the observed value is very good. This is probably as low a β value as one can obtain in any of the stabilized structures based on SiO_4 tetrahedra. The next best simple structure may be $HfSiO_4$ where $\bar{\beta} \simeq 3.8 \times 10^{-6}/°K$. Here the anisotropy in β is $\Delta\beta \simeq 2 \times 10^{-6}/°K$, and it may cause microcracking during thermal cycling.

There has been some thought that the X_1 phase in the Si-Al-O-N quaternary system might be useful. The X_1 phase has $\beta=3.6 \times 10^{-6}/°K$ (Ref. 37), which is comparable to mullite. Although the structure of X_1 has not been worked out, it probably contains some octahedral Al since the oxygen to nitrogen ratio is about 3:1. Thus the thermal expansion and other properties are probably similar to mullite. It does not appear to be a better window candidate than mullite.

The good window candidate with SiO_4 groups in them are believed to be (see Table 21)

Mullite	$Al_6Si_2O_{12}$
Pollucite	$CsAlSi_2O_6$
Willemite	Zn_2SiO_4
Sialon	$SiAl_2O_2N_2$
Hafnon	$HfSiO_4$

The germanium analogs of some are also good candidates.

V. Other Tetrahedral Units

The BO_4, BeO_4, and PO_4 units have optical vibration frequencies near to or higher than that of the SiO_4 units. There appears to be no great advantage in using these compared to the silicates. The vibration frequencies of AlO_4, GaO_4, and GeO_4 are somewhat lower than those of SiO_4 so that the infrared pass band is greater. What compounds can be made from these? The crystal chemistry problems of GeO_4 are similar to those of SiO_4, hence the resolution of them is similar. The recommended compounds for GeO_4 are

TABLE 21: Useful Binary Oxides and Nitrides

First Cation \ Second Cation	Z=3 η=4	Z=4 η=4	Z=5 η=4	Z=5 η=6
Z=2 η=4	$CdAl_2O_4$ $CaAl_4O_7$ $SrAl_4O_7$	$BeSiN_2$ Zn_2SiO_4 Zn_2GeO_4		
Z=3 η=4	$Al_{18}B_4O_{33}$	$Al_6Si_2O_{13}$ $Al_6Ge_2O_{13}$ $CsAlSi_2O_6$ $Al_2SiO_2N_2$ $Al_2GeO_2N_2$?		
Z=3 η=6	$Al_{18}B_4O_{33}$ (a)	$Al_6Si_2O_{13}$ $Al_6Ge_2O_{13}$	$ScNbO_4$ $ScTaO_4$	
Z=4 η=6				$TiTa_2O_7$? $TiNb_2O_7$?
Z=5 η=6				$NbPO_5$? $TaPO_5$?
Z=4 η=8		$ZrSiO_4$ $HfSiO_4$ $ThGeO_4$		

(a) When a compound occurs in more than one box, it means that the cation occurs in more than one kind of site.

Thorium Germanate (zircon structure)	$ThGeO_4$
Germanium Mullite	$Al_6Ge_2O_{13}$
"Gealon"	$GeAl_2O_2N_2$

The last compound in this list may or may not exist. If it does exist, it should have a low thermal expansion.

The crystallographic problems of AlO_4 and GaO_4 are different from those of SiO_4. Both Al^{3+} and Ga^{3+} are sufficiently larger in size than Si^{4+} that they often occur in $\eta=6$ sites instead of $\eta=4$ sites. The method of inducing these Z=3 ions into $\eta=4$ sites is to construct compounds with other metal oxides which customarily have $\eta \geq 6$ and also have low β values. The first thought is to use Z=5, $\eta=6$ ions such as Ta^{5+}, Nb^{5+}, or V^{5+}. Unfortunately the $AlTaO_4$, $AlNbO_4$, $GaNbO_4$ have all of the metal atoms in $\eta=6$. The β values are, thus, not very small. In $AlVO_4$ and $GaVO_4$ both atoms have $\eta=4$, and these compounds possess all of the instabilities of SiO_2 and $AlPO_4$.

The next choice for compounds is with Z=4, $\eta=6$ ions yielding only Al_2TiO_5. This compound is unstable below 1150°C and has a highly anisotropic thermal expansion. The Al coordination is midway between $\eta=4$ and 6. For Z=3 ions we have $Al_{18}B_4O_{13}$, a good candidate where the B has $\eta=4$ and the Al presumably has $\eta=4$ and 6. Another Z=3 compound, $Sc_2Al_8O_{15}$, exists with a melting point of 1850°C. The structure is unknown. If the Al all has $\eta=4$, then the β should be β(est.) $\sim 3 \times 10^{-6}$/°K. If the Al all has $\eta=6$, then β(est.) $\sim 9 \times 10^{-6}$/°K. Since Al has $\eta=6$ in $YAlO_3$, $LaAlO_3$, and both $\eta=4$ and $\eta=6$ in $Y_2Al_5O_{12}$, it seems unlikely that $Sc_2Al_8O_{15}$ will have $\eta=4$ for Al. Thus it is not useful as a low β material.

Compounds with Z=2, $\eta \geq 4$ exist with Al_2O_3. With Be, Mg, Zn the Al has $\eta=6$. With Cd one obtains $CdAl_2O_4$ with $\eta=4$ for both ions, this might be useful. Two other good examples of $\eta=4$ are $CaAl_4O_7$ and $SrAl_4O_7$. In both the Al has $\eta=4$ while the Ca and Sr have $\eta=12$. The $CaAl_4O_7$ is known to have low thermal expansion (Ref. 39). These two materials deserve further study. Compounds with Z=1 ions such as $LiAlO_2$, $RbAlO_2$, $CsAlO_2$ may have low expansion. The K, Rb, and Cs compounds are too hygroscopic to be useful.

The crystal chemistry of GaO_4 is less well known than that of AlO_4. Both $CaGa_4O_7$ and $SrGa_4O_7$ exist, their structures are unknown. They may also have low expansion coefficients.

VI. Stabilization of Other Tetrahedral Units

We have dealt with nitrogen stabilization of Si-Al-O-N compounds. There does not appear to be any very useful AlO_xN_y compounds with all tetrahedral Al. The next choice is to go the carbon stabilization. There exist two compounds Al_4O_4C and Al_2OC. In both of these the Al is in tetrahedral coordination. In Al_2OC the tetrahedra are AlO_2C_2. The expansion behavior of an AlC_4 tetrahedron can be estimated from a comparison of SiC_4, SiN_4, and AlN_4 tetrahedra. The estimate is $\beta \simeq 7.5 \times 10^{-6}/°C$. The AlO_4 tetrahedron has $\beta \simeq 1 \times 10^{-6}/°C$. Thus the AlO_2C_2 should have an average value of $\beta \simeq 4.3 \times 10^{-6}/°C$. This is not sufficiently low to be interesting. The Al_4O_4C has AlO_3C tetrahedra. Here the estimated expansion coefficient is $\beta \simeq 3.5 \times 10^{-6}/°K$. This begins to make Al_4O_4C an interesting candidate material, and it should be pursued.

We could attmept to find binary oxides using Z=2, η=4 oxides such as BeO and ZnO as a base. The fundamental thermal expansion of BeO_4 and ZnO_4 makes this unattractive. Two exceptions, already mentioned, are Zn_2SiO_4 and Zn_2GeO_4.

There are also tetrahedra with Z=5 in such compounds as $AlPO_4$, $AlAsO_4$, $AlVO_4$, $ScPO_4$, $ScVO_4$, $ScNbO_4$, $ScTaO_4$, YPO_4, YVO_4, $YNbO_4$, and $YTaO_4$. The first three have unstable quartz-like structures and are not considered further. The $ScPO_4$ and $ScVO_4$ have zircon ($ZrSiO_4$) structures; the $ScNbO_4$ and $ScTaO_4$ have $NiWO_4$ structures; the YPO_4 and YVO_4 have scheelite ($CaWO_4$) structures. The thermal expansion anisotropy of all of the measured scheelite structures is very large, so these are not useful. This leaves $ScVO_4$, $ScNbO_4$, $ScTaO_4$ as possible candidates. In $ScNbO_4$ and $ScTaO_4$ the Sc has Z=3, η=6. The estimated thermal expansion, produced mostly by the Sc^{3+}, is $\beta \simeq 5 \times 10^{-6}/°K$. Even though this value is rather high, it is about one half that of Sc_2O_3 and Y_2O_3. Since $ScNbO_4$ and $ScTaO_4$ should have infrared pass bands comparable to Sc_2O_3 and Y_2O_3 in wavelength regions of crucial importance, they look like useful candidates.

No thermal or optical data on them are yet available to test this hypothesis.

The tetrahedral units MoO_4 and WO_4 with Z=6 for Mo and W exist. These are found in such compounds as Li_2WO_4, $CdWO_4$, $ZnWO_4$, $Sc_2W_3O_{12}$, $Sc_2MO_3O_{12}$, $Al_2W_3O_{12}$. In Li_2WO_4 the Li^{1+} has η=4, in the others the metal atoms, Cd, Zn, Sc, Al, have η=6. In $SrWO_6$, $CaMoO_4$ the metal coordiantion for Sr etc is η=8. The lowest estimated expansion of all is for $Al_2W_3O_{12}$ with β(est.) $\simeq 3.6 \times 10^{-6}$/°K. Measurements by Martinek and Hummel (Ref. 40) on ceramic give $\beta \simeq 2 \times 10^{-6}$/°K. This structure has a pronounced (010) cleavage, so expansion anisotropy and microcracking are apt to be a problem. No work is recommended at present on any of these six compounds.

Compounds of W^{6+} with Zr^{4+} or Hf^{4+} do exist as ZrW_2O_8 and HfW_2O_8; there are no Ti^{4+}-W^{6+} oxide compounds. These compounds are unstable below 1100°C and should be avoided, even though ceramic bodies do have low thermal expansion (Ref. 40). Again, one has the problem of too many oxygen atoms per metal atom to make stable crystal structures. This appears to exhaust the possibilities of units with η=4.

VII. Stabilization of Octahedral Units

The thermal expansion coefficients of η=6 units of Nb^{5+}, Ta^{5+}, Ta^{5+}, and Sn^{4+} in Table 18 is $\beta \simeq 3$ to 4×10^{-6}/°K. These values are much lower than for other η=6 units where Z=2 or 3. These simple oxides SnO_2, Ta_2O_5, Nb_2O_5 do not have useful properties as window materials by themselves. Can we find binary oxides of low expansion with improved properties? The crystal stabilization problem for Ta_2O_5 and Nb_2O_5 is similar to that in SiO_2; the oxygen/metal ratio is so high that the crystals tend to be unstable to deformation. This is especially true in WO_3. In WO_3 with η=6 one only obtains good crystals with the incorporation of Na in the η=12 sites between the WO_6 octahedra. The octahedra are all joined at their corners to only one other in the Na_xWO_3 or ReO_3 or AlF_3 crystal structure. The Na stabilizes the WO_3 structure and produces a low thermal expansion above 200°C (Refs. 31, 32). The high expansion coefficient of NaO_{12} is not exhibited because the W-O

framework encages the Na ions and prevents their expansion from taking place. So in this case as in the pollucite the framework structure encages the high expansion alkali ions. The same is true in $KNbO_3$ where $\beta=4 \times 10^{-6}/°K$ (Ref. 25-Megaw). Here the expansion is determined by the Nb-O framework. The total β is thus <u>not</u> the sum of the β of the individual component ion groups, it is less. The $\beta = 4 \times 10^{-6}/°K$ is close to that for the NbO_6 groups themselves. There may be other examples of such behavior among the compounds $MgTa_2O_6$, $CaTa_2O_6$, $SrNb_2O_6$, $CaTa_4O_{11}$ etc. More work here is needed to choose useful candidates.

Of the various stabilized compounds of Nb^{5+} and Ta^{5+} there are only two that appear to be promising with Z=4 oxides. These are $TiNb_2O_7$, and $TiTa_2O_7$. They have melting points above 1350°C, they should be transparent to the infrared out to wavelengths of 5 microns and have $\beta \leq 4 \times 10^{-6}/°K$. Measurements of β for the Ti compounds have given (Ref. 40) polycrystalline average values of $\beta=2.3 \times 10^{-6}/°K$ for $TiNb_2O_7$ and $3.4 \times 10^{-6}/°K$ for $TiTa_2O_7$. These titanates are monoclinic. If the expansion anisotropy is small and the oxide ceramics strong, they could be very useful. However, it is believed that they are weak, soft, and anisotropic. The niobates and tantalates of Al^{3+} and Sc^{3+} have already been mentioned, $ScNbO_4$ may be useful. Two other compounds of high stability and unknown utility are $NbPO_5$ and $TaPO_5$.

A search of the available literature revealed no useful binary oxides with SnO_2.

VIII. Ternary Oxides

There may be several useful ternary oxides with low thermal expansion. The compound $CsAlSi_2O_6$, pollucite, has already been mentioned. Both beryl and cordierite, $Be_3Al_2Si_6O_{18}$ and $Mg_2Al_4Si_5O_{18}$, are ternaries. The pollucite is cubic but has low hardness, the other two are hexagonal and orthorhombic respectively and of moderately high hardness (1120 and 900 kg/mm^2). Unfortunately their thermal expansions are anisotropic, and this can cause trouble. Another

interesting candidate is rhodizite, $CsB_{12}Be_4Al_4O_{28}$, which is cubic, has high hardness (about 1600 kg/mm^2), and whose expansion is unknown. The estimated expansion, based on B and Be in η=4 sites and Al in η=6, is β(est.)$\simeq 4.5 \times 10^{-6}$/°K. If one could change the composition to $CsB_{12}Al_4Mg_4O_{28}$ with the Mg in the η=6 sites, the estimated expansion would be β(est.)$\simeq 3 \times 10^{-6}$/°K. For a cubic, hard, material this low expansion would be very desirable. Some work on this material in synthetic form is recommended.

IX. Summary of Recommended Materials

The simple binary compounds that are recommended for some study next year are AlN, BP, Y_2O_3, $ThO_2$and ZrO_2. These have been discussed in previous reports and their properties have been enumerated. None of these looks like the best possible candidate, but all have some special merit in terms of long-wavelength pass band, or high thermal conductivity, or cubic crystal structure.

The binary oxides (ternary compounds) that appear to be of interest are given in Table 21, arranged according to Z and η. The best candidates from Table 21 appear, as of today, to be (in order of preference) $Al_6Si_2O_{13}$, $Al_6Ge_2O_{13}$, $Al_{18}B_4O_{33}$, $Al_2SiO_2N_2$, $BeSiN_2$, Zn_2GeO_4, and $ThGeO_4$. Some exploratory work should be done on the others, particularly $CdAl_2O_4$, $SrAl_4O_7$, and $ScTaO_4$, in order to test their properties. The first three choices above should be worked on in the second year in order to find methods for making them optically translucent or transparent. Some work on densifying $BeSiN_2$ should also be done. Work on $Al_2SiO_2N_2$ should be started, particularly synthesis and hot pressing. Exploration of the others on a small scale is recommended. The compound Al_4O_4 looks enticing enough that some exploratory work on this should be carried out. Some exploratory work on $CsB_{12}Be_4Al_4O_{28}$ is clearly needed.

There may be other ternary oxides of the type M-Al-Ge-O, M-Al-Ga-O, M-Ga-Ge-O where M is some large cation such as Ca, Sr, Ba, La, or Lu. Very little literature data exist for these systems, and work would have to be selective. These oxides should, however, have the advantage of transmitting in the visible and near infrared out to 5 microns.

References for Section 5.0

Oxide Expansion References

1. N. Soga, J. Am. Ceram. Soc. 47, 469 (1964).

2. A Correction for the Expansion of the Second Ion In Its Own Coordination Has Been Made.

3. G. A. Slack and S. F. Bartram, J. Appl. Phys. 46, 89 (1975).

4. G. Bayer, J. Less-Common Met. 26, 255 (1972).

5. F. P. Hall, J. Am. Ceram. Soc. 13, 182 (1930); and G. W. Morey "Properties of Glass", Reinhold, New York, 1954, Second Ed. p 272; and T. A. Hahn and R. K. Kirby, A. I. P. Conf. Proc. 3, 13 (1971)

6. G. K. White and O. L. Anderson, J. Appl. Phys. 37, 430 (1966).

7. E. P. Meagher, Am. Mineral. 60, 218 (1975).

8. Y. S. Touloukian et al, "Thermophys. Prop. Matter", vol 13,Plenum, NY (1977).

9. J. B. Wachtman Jr., T. G. Scuderi, and G. W. Cleek, J. Am. Ceram. Soc. 45, 319 (1962).

10. H. Ito, K. Kawada, and S. Akimoto, Phys. Earth Planet. Inter. 8, 277 (1974).

11. Z. P. Chang and G. B. Barsch, IEEE Trans. Sonics Ultrason. SU23, 127 (1976).

12. F. A. Hummel, J. Am. Ceram. Soc. 32,320 (1949).

13. O. Kamada, T. Takizawa, and T. Sakurai, Jap. J. Appl. Phys. 10, 485 (1971).

14. K. M. Merz, W. R. Brown, and H. P. Kirchner, J. Am. Ceram. Soc. 45, 531 (1962)

15. L. J. Eckert and R. C. Bradt, J. Am. Ceram. Soc. 56, 229 (1973).

16. M. K. Murthy, J. Am. Ceram. Soc. 45, 616 (1962).

17. K. V. K. Rao, S. V. N. Naidu, and L. Iyengar, J. Am. Ceram. Soc. 51, 467 (1968).

18. Kh. S. Bagdasarov, S. E. Salibekov, and V. S. Krylov, Neorg. Mater. 6, 1538 (1970)[Inorg. Mater. 6, 1356 (1970)].

19. H. Ibach, Phys. Status Solidi 33, 257 (1969).

20. S. Nanamatsu, K. Doi, and M. Takahashi, Jap. J. Appl. Phys. 11, 816 (1972).

21. P. Y. Wen, J. J. Brown, and F. A. Hummel, Trans. Brit. Ceram. Soc. 63, 501 (1964).

22. R. J. Beals and R. L. Cook, J. Am. Ceram. Soc. 40, 279 (1957).

23. D. W. Stacy and D. R. Wilder, J. Am. Ceram. Soc. 56, 224 (1973); and C. E. Curtis, J. Am. Ceram. Soc 40, 274 (1957).

24. O. J. Whittemore Jr. and N. N. Ault, J. Am. Ceram. Soc. 39, 443 (1956).

25. G. L. Dwivedi and E. C. Subbarao, J. Am. Ceram. Soc. 56, 443 (1973); W. R. Manning, O. Hunter Jr., F. W. Calderwood, and D. W. Stacy, J. Am. Ceram. Soc. 55, 342 (1972); H. D. Megaw, Acta Cryst. 24A, 589 (1968).

26. H. P. Singh and B. Dayal, Solid State Commun. 7, 725 (1969).

27. K. D. Kundra and S. Z. Ali, J. Appl. Cryst. 3, 543 (1970).

28. A. Eisenstein, J. Appl. Phys. 17, 434 (1946); R. J. Zollweg, Phys. Rev. 100, 671 (1955).

29. E. M. Dudnik, G. V. Lashkarev, Yu. B. Paderno, and V. A. Obolonchik, Neorgan, Mater. 2, 980 (1966) [Inorgan. Mater. 2, 833 (1966)].

30. M. L. Gupta and S. Singh, J. Am. Ceram. Soc. 53, 663 (1970); S. Stecura and J. W. Campbell, U. S. Bur. Mines Report of Investig. #5847 (1960).

31. C. Rosen, B. Post, and E. Banks, Acta Cryst. 9, 475 (1956).

32. T. Takamori and M. Tomozawa, J. Am. Ceram. Soc. 47, 472 (1964).

33. M. Hoch and A. C. Momin, High Temp. High Press. 1, 401 (1969).

34. C. M. B. Henderson and D. Taylor, Trans. J. British Ceramic Soc. 74, 49 (1975).

35. E. Edjer, Phys. Status Solidi A23, K87 (1974).

36. A. U. Sheleg and V. A. Savastenko, Vestsi Akad. Navuk BSSR, Ser. Fiz. Mat. Navuk (#3), 126 (1977) [Chem. Abstr. 85, 169929a (1976) and 87, 73467p (1977)].

37. J. P. Dismukes, W. M. Yim, and V. S. Ban, J. Cryst. Growth 13/14, 365 (1972).

38. L. J. Gauckler, S. Prietzel, G. Bodemer, and G. Petzow in "Nitrogen Ceramics", Ed. F. L. Riley, Noordhoof, Leyden, 1977, p. 529.

39. E. Criado, S. DeAza, and D. A. Estrada, Bol. Soc. Esp. Ceram. Vidrio 14, 271 (1975).

40. S. R. Skaggs, Los Alamos Scientific Laboratory Report LA-6918-MS (Sept. 1977).